Numerical simulation of magnetic islands in tokamak plasmas

Hashimoto, Ryohei
Interdisciplinary Graduate School of Engineering Sciences, Kyushu University

Yagi, Masatoshi
Research Institute for Applied Mechanics, Kyushu University

Nishimura, Seiya
Interdisciplinary Graduate School of Engineering Sciences, Kyushu University

Itoh, Sanae-I.
Research Institute for Applied Mechanics, Kyushu University

https://doi.org/10.15017/27059

出版情報：九州大学応用力学研究所所報. 137, pp.117-136, 2009-09. Research Institute for Applied Mechanics, Kyushu University
バージョン：
権利関係：

Numerical simulation of magnetic islands in tokamak plasmas

Ryouhei HASHIMOTO*1, Masatoshi YAGI*2, Seiya NISHIMURA*1 and Sanae-I. ITOH*2
E-mail of corresponding author: *ryouhei@riam.kyushu-u.ac.jp*

(Received June 1, 2009)

Abstract

The neoclassical tearing mode (NTM), which is a possible candidate to drive magnetic island, is the tearing mode nonlinearly driven by the perturbed bootstrap current via neoclassical electron viscosity under the condition of $\Delta' < 0$, where classical tearing mode is stable. The diamagnetic drift stabilizes the tearing mode and gives rise to finite rotation frequency. Furthermore, the diamagnetic rotation frequency of magnetic island plays quite important role for the nonlinear stability of NTM. Therefore, effects of the neoclassical electron viscosity on the drift-tearing mode should be investigated. In this study, we examine effects of the neoclassical electron viscosity(the perturbed bootstrap current) on the drift-tearing mode numerically and analytically.

Key words : *magnetic island, neoclassical electron viscosity, bootstrap current, drift-tearing mode*

1. Introduction

Modern society has been developed by science and technology, which heavily depend on fossil fuels such as petroleum, coal, gas and so on. As the result, the world-wide demand for energy has been increasing rapidly. It is expected that more energy will be consumed according to an explosive increase of the world population in the near future. Environmental destruction and global warming are crucial issues to be resolved.

Nuclear fusion energy is expected as one of alternatives to fossil fuel. The most promising way is nuclear fusion of Deuterium and Tritium, in which Alpha particle and neutron are produced[1]. In this process, there is no production of greenhouse gasses. High temperature heated plasmas of Deuterium and Tritium are necessary to realize the nuclear fusion, and this method is called the controlled thermonuclear fusion. Magnetic Confinement Fusion (MCF) such as tokamaks is one of candidates for nuclear fusion reactor. Over the past fifty years, main effort has been devoted to heat up the plasmas, where a target value of plasma temperature is one hundred million degrees Kelvin[1]. In the International Thermonuclear Experimental Reactor (ITER) project, it is expected that the long time self-sustainment of nuclear fusion will be achieved[2].

High temperature magnetized plasmas are potentially unstable, because of their various instabilities driven by gradients of plasma temperature, density and electric current. In the plasma core region, there exist micro-turbulence and macroscopic magnetohydrodynamic (MHD) instability[1]. Micro-turbulence enhances transports of energy and particles, which are attributed to the confinement degradation. Excitation of MHD instability strongly modifies equilibrium fields, and sometimes it causes the disruption[3,4]. The simultaneous achievement of high temperature and dense plasmas suppressing instabilities is still a challenging problem.

Magnetic islands, which often appear at rational surface where parallel wave number is zero, are the typical example of the MHD instability in tokamaks. The degradation of plasma confinement has been observed, when the magnetic island width becomes larger enough[5]. The bootstrap current is a self-generated plasma current driven by the pressure gradient, which is an important factor for the design of economically efficient nuclear fusion reactors[2]. One of the destabilization mechanism of magnetic islands is associated with the loss of bootstrap current, owing to the flattening of pressure gradient by magnetic islands. As the results, it enhances the transport of heat and particles. Besides,

*1 Interdisciplinary Graduate School of Engineering Sciences, Kyushu University
*2 Research Institute for Applied Mechanics, Kyushu University

the disruption, a sudden collapse of plasma discharge accompanying a large current flow in vacuum vessel, is occasionally triggered by the magnetic islands, and causes serious damages on devices[1,6]. It is desired to control the magnetic island dynamically and/or suppress their excitations. In the ITER project, the excitation of magnetic islands might be suppressed by using electron cyclotron current drive (ECCD)[2,7].

Although much work has been done on magnetic island problems, some important issues still remain unresolved.

The neoclassical tearing mode (NTM), which is a possible candidate to drive magnetic island, is the tearing mode nonlinearly driven by the perturbed bootstrap current via neoclassical electron viscosity under the condition of $\Delta' < 0$, where classical tearing mode is stable. The Rutherford type equation is derived to analyze NTM, and the sub-critical excitation of magnetic island is possible if the transport threshold is taken into account. The tearing mode combined with electron diamagnetic drift effect with $\Delta' > 0$, where classical tearing mode is unstable, is known as the drift-tearing mode. The diamagnetic drift stabilizes the tearing mode and gives rise to finite rotation frequency. Furthermore, the diamagnetic rotation frequency of magnetic island plays quite important role for the nonlinear stability of NTM. Therefore, effects of the neoclassical electron viscosity on the drift-tearing mode should be investigated. In this study, we examine effects of the neoclassical electron viscosity(the perturbed bootstrap current) on the drift-tearing mode numerically and analytically.

The present thesis is organized as follows. In Chapter 2, the fundamental basis of the present study is introduced. Some of important physics issues in ITER and theory of magnetic islands are reviewed. In Chapter 3, model equations are introduced. A reduced set of two-fluid equations are derived. In Chapter 4, the linear stability analysis of the drift-tearing mode is performed. The destabilization mechanism of the drift-tearing mode with the neoclassical electron viscosity is clarified. Furthermore, the nonlinear simulations are performed and the saturation mechanism of the magnetic island is investigated. In Chapter 5 is devoted for summary and discussion.

2. Review

2.1 Important subjects in ITER

The purpose of the International Thermonuclear Experimental Reactor (ITER) project is to achieve the self-ignition and the self-sustainment of the burning state by the α-particle heating power[2]. The main goal of ITER project is to obtain the experimental data, which is necessary to construct the subsequent demonstrative fusion power plant. For the high performance of burning plasmas, high-β states and long confinement times are necessary efficiently utilizing H modes and internal transport barriers, which can be realized by avoiding magneto-hydrodynamics (MHD) instabilities and by suppressing turbulent transport by means of magnetic shear and zonal flow[10] for the suppression of turbulence transport. The parameter regime of ITER operation is determined both by economical reasons, and by some serious issues as discussed below.

Disruption is a sudden loss of magnetic confinement, followed by a rapid cooling (thermal quench) and current loss (current quench) of plasmas. Rapid loss of thermal energy causes the plasma temperature to fall to as low as 3 eV, which is expected to occur on 1 ms in ITER[2]. Subsequent loss of plasma current induces strong current flows in the vacuum vessel on the 50 ms. Consequent damages on devices are deposition of thermal energy onto the divertor, melting of plasma facing materials and strong electromagnetic forces on devices (15,000 t in the most sever cases).

It is generally accepted that the thermal quench is initiated by the growth of large amplitude magnetic islands in many cases. It has been pointed out that magnetic island growth is triggered by the locking of poloidal rotation (zero rotation frequency) of magnetic island, which is caused by the interaction with resistive wall following eddy current[11,12]. The locked magnetic island also degrades the confinement property by affecting the edge transport (H-mode) barrier. When the magnetic island width overcomes a threshold, the magnetic islands with different mangetic helicities overlap on rational surfaces. The overlap produces large scale ergodization of the magnetic structure and enhances conductive transport of thermal energy along ergodized magnetic field lines[13,14]. In other cases, the disruption is caused by the β-limit or the density (Greenwald) limit. Ideal MHD instability such as the kink mode and the ballooning mode becomes unstable with sufficiently large β value. The physics mechanism of the density limit is presently not yet clear, however it is considered to be triggered by the radiative instabilities when the density at plasma edge becomes large enough.

Minor repetitive collapse events (partial disruptions) are known as the sawtooth oscillation and the edge localized mode (ELM), for example, and they are essentially relaxation of equilibrium profiles accompanying intermittent energy releases. The sawtooth oscillation occurs in the core region, therefore it does not affect the global energy confinement. However, the sawtooth oscillation often triggers the excitation of magnetic island[15]. Dynamics of ELM associated with H-mode confinement is

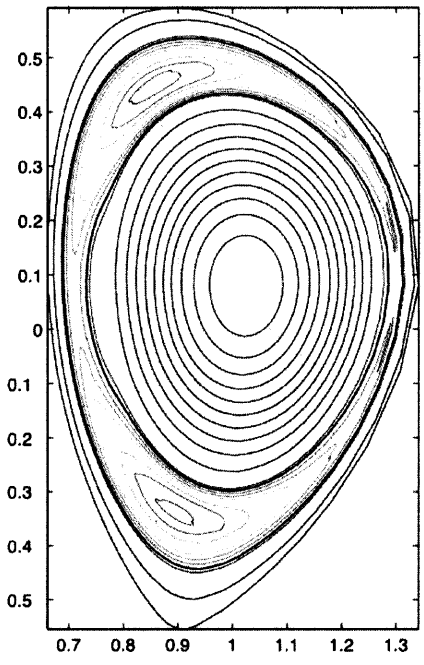

Fig. 1 Simulation of the worst case (maximal size) for magnetic islands in ITER(quoted from Ref.[2]).

just beginning to be described theoretically. ELM activity can be categorized into some types, and control of them is important for saving plasma facing components and steady operation of ITER.

2.2 Magnetic islands in ITER

The scaling with the experimental data gives a threshold width for the onset of magnetic islands such that $2-7$ cm in ITER[2]. This is a few percent of the minor radius, and it is considered to be difficult to avoid the excitation of magnetic islands. Fig.1 shows estimated magnetic island structure in ITER with a contour of magnetic field in the poloidal cross section.

The important issues concerning magnetic islands for ITER and also future tokamak power plants are summarized as follows.

- **Trigger mechanism and threshold width:**
  The seeding process for excitation of magnetic islands should be clarified. Moreover, the detailed physics mechanism which determines threshold width of magnetic island excitation is undergoing subject. In order to check two representative mechanisms, i.e. the transport threshold mechanism (by Fitzpatrick)[8] and the polarization current threshold mechanism (by Smolyakov)[9], further investigations are necessary. Current experimental data implies that both models are plausible.
- **Saturated width:**
  Estimation of saturated magnetic island is quite important to determine the influences on confinement. A stable and stationary solution of the modified Rutherford equation gives a saturated width[16].
- **Effects on confinements:**
  In connection with trigger of disruption, investigations are necessary on the locking of rotation of magnetic island by resistive wall, on the consequent interaction between magnetic island and edge transport barrier and on the overlap of magnetic islands. The limitation of achievable β value caused by magnetic islands is also an important subject.
- **Methods for avoiding onset and controlling growth:**
  The electron cyclotron current drive, which replaces the missing bootstrap current inside magnetic island is planned to be employed to stabilize magnetic islands in ITER. Recently, current/safety factor profile modifications have been used to improve plasma confinement. Perturbed bootstrap current can be changed to stabilizing contribution in the reversed magnetic shear region.

2.3 Tearing mode

The linear stability analysis of the tearing mode was originally given by Furth, Kleen and Rosenbluth[17], which is based on the boundary layer theory around the rational surface. The growth rate of the linear tearing mode is obtained by matching the ideal MHD solution for the outer layer and the resistive MHD solution for the inner layer. The ideal MHD solution is characterized by the parameter Δ', which represents the logarithmic jump of the radial magnetic field perturbation across the rational surface:

$$\Delta' = \frac{\tilde{\Psi}'(r_s+0) - \tilde{\Psi}'(r_s-0)}{\tilde{\Psi}(r_s)} \tag{1}$$

where $\tilde{\Psi}$ is fluctuating flux function (vector potential), r_s is position of the rational surface. The tearing mode is unstable, when Δ' is positive. Assuming that the perturbation grows as $e^{\gamma t}$, the linear dispersion relation is given by

$$\gamma^5 = \left(\frac{1}{2\pi}\frac{\Gamma(1/4)}{\Gamma(3/4)}\right)\left(\frac{R_0}{v_A}\right)^2 (r_s R_0 k_\parallel')^2 \tau_R^{-3} (r_s\Delta')^4, \tag{2}$$

with

$$\tau_R = \frac{4\pi r_s^2}{\eta_\parallel c^2} \tag{3}$$

where $k_\parallel$ is the wave number along the magnetic field line and the prime indicates the radial derivative. τ_R is resistive time, where $\eta_\parallel$ is parallel resistivity and c is

velocity of light. R_0 is major radius of plasmas. v_A indicates Alfvén velocity. It has been recognized that the characteristics (dispersion relation) of the tearing mode is changed, according to the collisionality of plasmas: the collisional tearing mode, the semi-collisional tearing mode and the collisionless tearing mode[18]. The above dispersion relation Eq.(2) corresponds to the collisional tearing mode.

An important extension of the tearing mode is the drift-tearing mode, which includes the effect of the electron diamagnetic drift. The density gradient gives the (diamagnetic drift) rotation frequency to the tearing mode. The linear dispersion relation of the collisional drift-tearing mode is given by

$$\omega^2(\omega-\omega_{*n})^3 = i\left(\frac{1}{2\pi}\frac{\Gamma(1/4)}{\Gamma(3/4)}\right)\left(\frac{R_0}{v_A}\right)^2(r_sR_0k_\parallel')^2\tau_R^{-3}(r_s\Delta')^4, \quad (4)$$

where the $\omega_{*n} = c\beta_p v_A k_\theta/\omega_i L_n$ indicates the electron diamagnetic drift frequency. β_p is the poloidal plasma beta value, k_θ is poloidal wave number, ω_i is ion plasma frequency and $L_n = -n_{0s}/n_{0s}'$ is electron density gradient length, where n_{0s} is equilibrium electron density at rational surface and the prime indicates the radial derivative. Real and imaginary parts of ω correspond to the rotation frequency and the growth rate, respectively. Phase diagram for separating the tearing mode and the drift-tearing mode in the collisional and semi-collisional regime is shown in Fig.2[19] (diagram in Ref.[18] is also available). $C = 0.51(\nu_{e,i}/\omega_{*n})(m_e/m_i)L_q/L_n$ and $\hat{\beta} = \beta_p(L_q/L_n)^2$ represent a collisional parameter and a pressure parameter, where $\{\nu_{e,i}, m_e/m_i\}$ are electron-ion collision frequency and a ratio of electron inertia to ion inertia, respectively. $L_q = q_s/q_s'$ is magnetic shear length, where q_s is safety factor. In the collisionless regime, the fluid model is not relevant to be used so that the drift kinetic model is used for analyzing the collisionless tearing mode. It is predicted that the linear tearing mode of higher mode number is destabilized by the electron temperature[18]. These unstable modes are called the micro-tearing modes, in which the electron temperature gradient becomes an additional free energy source.

Analytical theory of the nonlinear evolution of the tearing mode was originally developed by Rutherford[16], and the time evolution of the magnetic island width is described by the so-called Rutherford equation:

$$I_1\frac{\tau_R}{r_s^2}\frac{\partial W}{\partial t} = \Delta', \quad (5)$$

with

$$W = 4\sqrt{\frac{q_sR_0}{s_sB_0}\tilde{\Psi}(r_s)}, \quad (6)$$

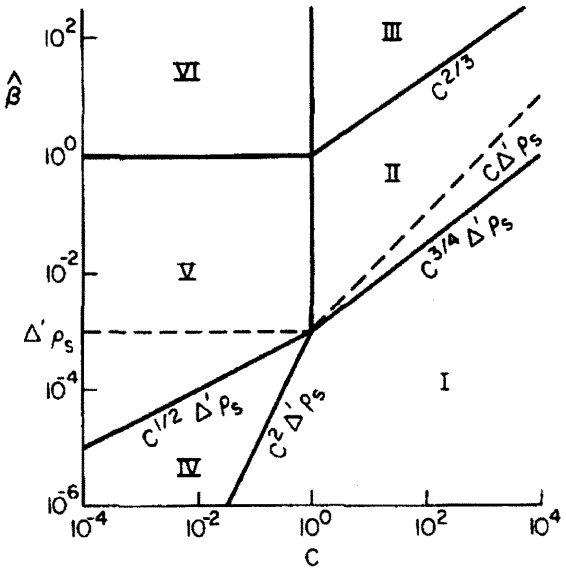

Fig. 2 Various regime of the tearing mode. In regions I and IV, the mode is purely growing and in regions II and V becomes the drift-tearing mode which is stable above the dashed line. The tearing mode no longer exists in region III and VI(quoted form Ref.[19]).

where $I_1 = 0.82$, W is the width of the magnetic island. s_s is the magnetic shear at the rational surface defined by $s_s = q_s'r_s/q_s$ and B_0 indicates the ambient magnetic field. The saturation of the tearing mode is given by $\Delta'(W) = 0$, which is caused by the quasi-linear modification of the equilibrium current profile inside magnetic island. By including this effect, the Rutherford equation is rewritten as

$$I_1\frac{\tau_R}{r_s^2}\frac{\partial W}{\partial t} = \Delta_0' - \alpha W. \quad (7)$$

where Δ_0' indicates the initial value of Δ' and α is a numerical parameter[20]. Saturated magnetic island width is given by $W_{\rm sat} = \Delta_0'/\alpha$ in the present model.

2.4 Neoclassical tearing mode

2.4.1 Classical and Neoclassical transports

The collisional transport in tokamak plasmas is mainly caused by the toroidal effect. Both particles and heat fluxes in the toroidal plasma are much lager than those in the cylinder one. In general, the transport in uniform and straight magnetic filed configurations is called as the classical transport, and that in the nonuniform and toroidal magnetic filed configurations is called the neoclassical transport. Firstly, we explain the classical transport.

In the fluid approximation, the transport of the plasma is caluculated by the simplificated Ohm's law and the balance equation of the pressure:

$$\mathbf{E} + \mathbf{v} \times \mathbf{B} = \eta \mathbf{j}, \tag{8}$$

$$\mathbf{j} \times \mathbf{B} = \nabla p. \tag{9}$$

Operating ($\times\mathbf{B}$) Eq.(8) and using Eq.(9), plasma flow across the magnetic filed line is given by

$$\mathbf{v}_\perp = -\eta \frac{\nabla p}{B^2} + \frac{\mathbf{E} \times \mathbf{B}}{B^2}. \tag{10}$$

The first term corresponds to the transport and the second term is $\mathbf{E} \times \mathbf{B}$ drift component. When the temperature is constant, the particle flux by the collision is given by

$$n\mathbf{v}_\perp^{\mathrm{col}} = -\frac{\eta\beta}{2\mu_0}\nabla n. \tag{11}$$

The diffusion coefficient D is defined as $\eta\beta/2\mu_0$, where $\beta = p/(B^2/2\mu_0)$. According to the resistive MHD theory, transports of particle and heat are enhanced by the $E \times B$ term of Eq.(10), and the flux of the particle given by Eq.(10) become $(1 + 2q^2)$ times larger where q is the safety factor. This enhancement is due to the distance across the magnetic surface, where larmor radius becomes larger in the toroidal coordinate.

Next, we discuss the so-called neoclassical transport. In the toroidal plasma, the collisional process is divided into three regions, the Pfirsch-Schlüter region, the banana region, the Plateau region, depending on the collisionality. In tokmak plasmas, magnetic field B is given by

$$B = \frac{B_0}{(1 + \epsilon + cos\theta)} \sim B_0(1 - \epsilon cos\theta), \tag{12}$$

where $\epsilon = a/R_0$ is the inverse aspect ratio. The particle is trapped in the weak magnetic field region, when the condition below is satisfied.

$$\left(\frac{v_\perp}{v_\parallel}\right)^2 > \frac{R_0}{R_0 + a}, \tag{13}$$

where $v_\parallel$ and $v_\perp$ are the parallel velocity and the perpendicular velocity. Alternatively, we obtained

$$\frac{v_\perp}{v_\parallel} \gtrsim \frac{1}{\epsilon^{1/2}}. \tag{14}$$

In order for the trapped particle to draw the banana orbit, the effective collision time τ_{eff} should be longer than τ_b, a time for rounding in the banana orbit. τ_b is estimated as

$$\tau_b \approx \frac{R}{v_\parallel}\left(\frac{2\pi}{\iota}\right) = \frac{R}{v_\perp \epsilon^{1/2}}\left(\frac{2\pi}{\iota}\right), \tag{15}$$

where ι is the rotational transform angle. ν_{eff} is approximately given by

$$\nu_{eff} = \frac{1}{\epsilon_t}\nu_{ei}, \tag{16}$$

where ν_{ei} is the collision frequency of the electron and ion. Therefore, the condition $\nu_{eff} < 1/\tau_b$ becomes

$$\nu_{ei} < \nu_b \equiv \frac{v_\perp \epsilon_t^{3/2}}{R}\left(\frac{\iota}{2\pi}\right) = \epsilon^{3/2}\frac{1}{R}\left(\frac{\iota}{2\pi}\right)\left(\frac{\kappa T_e}{m_e}\right)^{1/2}. \tag{17}$$

This region is called banana region and the electron can draw the banana orbit. The width of the banana orbit Δ_b is estimated as

$$\Delta_\mathrm{b} = \frac{mv_\parallel}{eB_p} \approx \frac{mv_\perp}{eB}\frac{v_\parallel}{v_\perp}\frac{B}{B_p} \approx \rho\Omega_e\epsilon^{1/2}\frac{R}{r}\frac{2\pi}{\iota} = \left(\frac{2\pi}{\iota}\right)\epsilon^{-1/2}\rho\Omega_e. \tag{18}$$

where B_p, ρ and Ω_e are the poroidal magnetic filed, the rotational radius, the the electron cyclotron frequency, respectively. If only the trapped electron is considered, the diffusion caused by the trapped particle is given as

$$D_{\mathrm{G.S.}} = \epsilon^{1/2}\Delta_\mathrm{b}^2\nu_{eff} = \epsilon^{1/2}\left(\frac{2\pi}{\iota}\right)^2\epsilon^{-1/2}(\rho\Omega_e)^2\frac{1}{\epsilon}\nu_{ei} \tag{19}$$

$$= \epsilon^{-3/2}\left(\frac{2\pi}{\iota}\right)^2(\rho\Omega_e)^2\nu_{ei}, \tag{20}$$

this is $\epsilon^{-3/2} = (R_0/a)^{3/2}$ times lager than the diffusion in the the large collisionality regime. This factor is derived by Galeev-Sagdeev, and $D_{\mathrm{G.S.}}$ is called the Galeev-Sagdeev diffusion coefficient.

2.4.2 Bootstrap current

When the plasma is in the banana region, it is predicted theoretically that the current in the toroidal direction is generated by the radial diffusion. This is called the bootstrap current, which is confirmed by experiments later. As described in the previous section, the electron draw the banana orbit for the case of $\mu_{ei} < \mu_b$. When there is the density gradient, the number of the banana particle passing the certain point and that coming close are different. The difference is $(dn_t/dr)\Delta_\mathrm{b}$. Since the velocity parallel to the magnetic field line of the trapped electron is $v_\parallel = \epsilon^{1/2}v_T$, where v_T is the thermal velocity. The current density is given by

$$j_\mathrm{bs} = -(ev_\parallel)\left(\frac{dn_t}{dr}\Delta_\mathrm{b}\right) = -\epsilon^{3/2}\frac{1}{B_p}\frac{dp}{dr}. \tag{21}$$

The passing electron drifts in the same direction by the collision with the trapped electron, and it is balanced by the collision with the ion. V_pass, which is the drift velocity of the passing electron in the steady state is written as

$$m_e V_\mathrm{pass}\nu_{ei} = \frac{\mu_{ee}}{\epsilon}m_e\left(\frac{j_\mathrm{bs}}{-en_e}\right), \tag{22}$$

where ν_{ee}/ϵ is the effective collision frequency. When the average velocity is taken into account, Eq(21) is

modified as

$$j_{\rm bs} \approx -\epsilon^{1/2} \frac{1}{B_p} \frac{dp}{dr}. \tag{23}$$

Using $\beta_p =< p > /(B_p^2/2\mu_0)$, which is the ratio of the average poloidal-beta, the ratio of the total bootstrap current I_b to the plasma current I_p is given by

$$\frac{I_b}{I_p} \sim c \left(\frac{a}{R}\right)^{1/2} \beta_p, \tag{24}$$

where $c \sim 0.3$. If β_p is large ($\beta_p \sim R/a$) and the pressure profile is precipitous, this value reaches a value close to unity.

2.4.3 The excitation of the neoclassical tearing mode

Time development of the nonlinear drift-tearing mode is described by the modified Rutherford equation combined with rotation frequency of magnetic islands (Scott and Hassam (1987))[21]). In order to close the equation, time evolution equation of rotation frequency is necessary.

In the high temperature plasmas, Δ' is estimated to be negative, although the excitation of the magnetic island is often observed in the high β regime. A magnetic island driven by the perturbed bootstrap current (neoclassical effect) is called the neoclassical tearing mode, where pressure gradient is an additional free energy source[22]. The modified Rutherford equation which includes effect of the perturbed bootstrap current is given as

$$I_1 \frac{\tau_R}{r_s^2} \frac{\partial W}{\partial t} = \Delta' + \Delta'_{\rm bs}, \tag{25}$$

with

$$\Delta'_{\rm bs} = I_2 \beta_p \sqrt{\frac{r_s}{R_0}} \frac{L_q}{L_p} \frac{1}{W}, \tag{26}$$

where $I_2 = 9.26$. $\Delta'_{\rm bs}$ indicates the perturbed bootstrap current contribution. $L_p = -p_{0s}/p'_{0s}$ is pressure gradient length at rational surface. If the neoclassical electron viscosity is interpolated for all collisionality regime, the model reduces to the Rutherford model in the Pfirsch-Schlüter regime. The effect of fluctuating bootstrap current is dominant in the collisionless so-called banana regime. Since the bootstrap current effect is proportional to $1/W$, a simple model predicts that the the neoclassical tearing mode is always unstable for small magnetic islands if $\Delta' < 0$. However, it was pointed out by Fitzpatrick[8]) that, considering the thermal transport effect, the perturbed bootstrap current contribution is modified as

$$\Delta'_{\rm bs} = I_2 \beta_p \sqrt{\frac{r_s}{R_0}} \frac{L_q}{L_p} \frac{W}{W^2 + W_d^2} \tag{27}$$

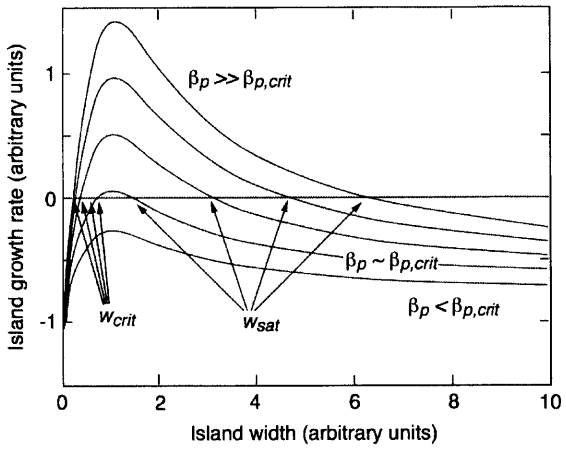

Fig. 3 Neoclassical tearing mode growth rate (dW/dt) versus magnetic island width(quoted form Ref.[2]).

with

$$W_d = 1.8 \sqrt{\frac{8R_0 L_q}{n}} \left(\frac{\chi_\parallel}{\chi_\perp}\right)^{1/4} \tag{28}$$

where $\{\chi_\parallel, \chi_\perp\}$ are parallel and perpendicular thermal transport coefficients and n is toroidal mode number. Therefore, the neoclassical tearing mode is unstable, only when the magnetic island width exceeds the critical size where the relation $\Delta' + \Delta'_{\rm bs} > 0$ is satisfied. The excitation mechanism of the neoclassical tearing mode is shown in Fig.3. $\beta_{p,crit}$ is the critical poloidal beta value for magnetic island excitation. $\{W_{crit}, W_{sat}\}$ indicate the threshold width and the saturation width. It is clearly shown that a seed island with finite size is necessary to excite large magnetic islands. This mechanism is called the transport threshold model.

Smolyakov has pointed out that the polarization current is an important factor to determine the threshold[9]). The polarization current is driven by the differential rotation between the magnetic island and the external flow. The effect of the polarization current is included such that

$$I_1 \frac{\tau_R}{a^2} \frac{\partial}{\partial t} W = \Delta' + \Delta'_{\rm bs} + \Delta'_{\rm pl}, \tag{29}$$

with

$$\Delta'_{\rm pl} = 4g \frac{L_q}{W^3} \frac{\omega_r (\omega_r - \omega_{*i})}{k^2 v_A^2}, \tag{30}$$

where $\Delta'_{\rm pl}$ indicates the polarization current contribution. g is a geometrical factor of order unity, ω_r is rotation frequency, k is wave number and $\omega_{*i} = -c\beta_p v_A k_\theta / \omega_i L_{pi}$ is ion diamagnetic drift frequency, where L_{pi} is ion pressure gradient length. The polarization current term gives rise to a new mechanism

of magnetic island excitation, i.e. polarization current threshold model, which modifies $\{W_{crit}, W_{sat}\}$ in Fig.3. The contribution of polarization current depends on the rotation frequency of magnetic islands. However, the widely accepted theoretical model which describes the time evolution of rotation frequency has not been obtained. Experiments show that the rotation frequency is in the range of $\omega_{*i} < \omega_r < 0$, therefore the polarization current has a stabilizing effect.

Two threshold models for the excitation of the neoclassical tearing mode are still under discussion.

3. Model equations

In order to derive model equations for the analysis of magnetic island dynamics, we start from two fluid equations for electron and ion. In this study, so-called Braginskii's two fluid equations are used, which are described in Appendix. The two-fluid equations include the fast frequency and small scale oscillation due to the compressional Alfvén dynamics as well as the low frequency and the large scale oscillation due to the shear-Alfvén dynamics. Therefore, it is convenient to construct the reduced set of model equations where only the shear-Alfvén dynamics is included in order to study the macroscopic low frequency shear-Alfvén dynamics. The compressional Alfvén dynamics can be excluded by the reduction scheme discussed in the following section.

Simplification

In order to avoid the complexity of the two-fluid system, simplifications are made. The cold ion limit is assumed, then the ion pressure is not solved. The ion anisotropic stress tensor is taken into account, but that of electron is neglected due to the mass ratio ordering. Electron inertia and neoclassical effects are neglected. The quasi-neutral condition is imposed for the ion and electron density such as $n_e = n_i = n$, so that only electron density evolution equation is solved. The external electron heat source, as well as the electron Ohmic heating, is not taken into account, i.e. $Q_e = 0$.

Then, simplified Braginskii's two-fluid equations are given such that:

$$m_i n \frac{d_i \mathbf{V}_i}{dt} = -\nabla P_e - \nabla \cdot \pi_i + \frac{1}{c}\mathbf{J} \times \mathbf{B}, \tag{31}$$

$$\mathbf{E} = -\frac{1}{en}\nabla P_e - \frac{1}{c}\mathbf{V}_e \times \mathbf{B} + \frac{1}{en}\mathbf{R}_{ie}, \tag{32}$$

$$\frac{d_e}{dt} n + n\nabla \cdot \mathbf{V}_e = 0, \tag{33}$$

$$\frac{3}{2} n \frac{d_e}{dt} T_e - T_e \frac{d_e}{dt} n = -\nabla \cdot \mathbf{q}_e, \tag{34}$$

where $\nabla \cdot \mathbf{V}_e$ in the electron continuity equation is substituted into that in the electron temperature equation. By introducing a vector potential $\mathbf{A}$ and an electric potential Φ, the magnetic field and the electric field are given by $\mathbf{B} = B_0\hat{\mathbf{z}} + \nabla \times \mathbf{A}$ and $\mathbf{E} = -\nabla\Phi - (1/c)\partial\mathbf{A}/\partial t$.

Shear Alfvén law

Operating $(\mathbf{B} \cdot \nabla\times)$ to Eq.(31), the so-call shear-Alfvén law is derived.

$$c\mathbf{B} \cdot (\nabla \times \mathbf{f} - 2\boldsymbol{\kappa} \times \mathbf{f}) = B^2 \mathbf{B} \cdot \nabla \left(\frac{J_\parallel}{B} \right) + 2c\mathbf{B} \times \boldsymbol{\kappa} \cdot \nabla_\perp P_e. \tag{35}$$

where $\mathbf{f} = m_i n (d\mathbf{V}/dt) + \nabla \cdot \pi_i$ and $\boldsymbol{\kappa} = (\mathbf{b} \cdot \nabla)\mathbf{b} = (4\pi/c)\mathbf{J} \times \mathbf{B}/B^2 + \nabla_\perp B/B$. The detailed derivation is given in Appendix.

Coordinate

In this thesis, a tokamak plasma with a major radius R_0 and a minor radius a is considered. We assume that an inverse aspect ratio $\epsilon = a/R_0$ is smaller than unity. In the reduction process, ϵ is used as an ordering parameter. The toroidal plasma can be described in the coordinate (R, ζ, Z), where R is the distance along major radius, ζ is the toroidal angle and Z is the vertical distance along the symmetry axis of toroidal coordinate. The (R, ζ, Z) coordinate is transformed into (x, y, z) coordinate such that $x = (R - R_0)/a$, $y = Z/a$, $z = -\zeta$. The ambient magnetic field is given by $B_0(x) = B_c/(1 + \epsilon x)$, where B_c indicates ambient magnetic field at the plasma center. The electron pressure is given by $P_e = nT_e$. In these coordinates, the spatial derivative is given by $\nabla = \hat{R}(\partial/\partial R) + \zeta(1/R)\partial/\partial\zeta + \hat{Z}\partial/\partial Z = (1/a)\{\hat{x}\partial/\partial x + \hat{z}\epsilon/(1 + \epsilon x)\partial/\partial z + \hat{y}\partial/\partial y\}$, where $1 + \epsilon x = R/R_0$ and unit vectors are $\hat{x} = \hat{R}$, $\hat{y} = \hat{Z}$ and $\hat{z} = -\hat{\zeta}$.

Ordering and normalization

We order each parameter with the inverse aspect ratio ϵ. Ordering is given by

$$\frac{\mathbf{V}_i}{v_A} \sim \epsilon, \quad \frac{\mathbf{V}_e}{v_A} \sim \epsilon, \quad \frac{c}{v_A}\frac{1}{B_c a}\Phi \sim \epsilon, \quad \frac{1}{B_c}\nabla \times \mathbf{A} \sim \epsilon, \quad \frac{4\pi}{B_c^2}(P_e - P_{ec}) \sim \epsilon, \quad \frac{4\pi}{B_c^2}\pi_i \sim \epsilon^2, \quad \frac{v_A}{R_0}t \sim \epsilon^{-1}, \tag{36}$$

where the suffix c indicates values at the plasma center. In this ordering, the ratio of strength of poloidal magnetic field to that of toroidal magnetic field is assumed to be $O(\epsilon)$. In addition, compressional Alfvén time is a/v_A and shear Alfvén time is R_0/v_A, where the Alfvén velocity is defined by $v_A^2 = B_c^2/4\pi n_c m_i$. The ratio of the resistive skin time $4\pi a^2/\eta_\parallel c^2$ to the shear-Alfvén time is assumed to be $O(\epsilon)$. Then, we define or replace values

such that:

$$\frac{\mathbf{V}_i}{v_A} \to \epsilon\mathbf{u}, \frac{\mathbf{V}_e}{v_A} \to \epsilon\mathbf{v}, \frac{c}{v_A B_c a}\Phi \to \epsilon\phi, \frac{\mathbf{A}}{aB_c} \to \epsilon\mathbf{A},$$
$$\frac{4\pi}{B_c^2}(P_e - P_{ec}) \to \epsilon p, \frac{4\pi}{B_c^2}\pi_i \to \epsilon^2\pi_i, a\nabla \to \nabla = \hat{x}\frac{\partial}{\partial x}$$
$$+ \hat{z}\frac{\epsilon}{1+\epsilon x}\frac{\partial}{\partial z} + \hat{y}\frac{\partial}{\partial y}, \frac{v_A}{a}t = \epsilon^{-1}t, \frac{v_A}{a}\frac{\partial}{\partial t} \to \epsilon\frac{\partial}{\partial t},$$
$$a\boldsymbol{\kappa} \to \boldsymbol{\kappa}, \frac{\mathbf{B}}{B_c} \to \mathbf{B}, \frac{4\pi}{c}\frac{a}{B_c}\mathbf{J} \to \mathbf{J}, \hat{z}\cdot\nabla_\perp \times \mathbf{A}_\perp \to B_\parallel,$$
$$A_\parallel = A, \frac{c}{v_A}\frac{1}{B_c}\mathbf{E} \to \mathbf{E} = -\epsilon\nabla\phi - \epsilon^2\frac{\partial \mathbf{A}}{\partial t},$$
$$a\frac{4\pi}{B_c^2}\mathbf{f} \to \mathbf{f} \to \epsilon^2\left(\frac{n}{n_c}\frac{d\mathbf{u}}{dt} + \nabla\cdot\pi_i\right), \frac{\eta_\parallel c^2}{4\pi a^2}\frac{a}{v_A} \to \epsilon\eta_\parallel,$$
$$\frac{\eta_\perp c^2}{4\pi a^2}\frac{a}{v_A} \to \epsilon\eta_\perp, \frac{1}{av_A}\frac{\kappa_{\parallel e}}{n_c} \to \epsilon\chi_\parallel, \frac{1}{av_A}\frac{\kappa_{\perp e}}{n_c} \to \epsilon\chi_\perp. \tag{37}$$

Even though $n/n_c \sim O(1)$ and $T_e/T_{ec} \sim O(1)$, we assume the fluctuation level of density and temperature is $O(\epsilon)$. If we operate some derivatives to n/n_c and T_e/T_{ec}, we expect that results are $O(\epsilon)$. Therefore, we order as $d_{i,e}(n/\epsilon n_c)/dt \sim O(1)$, $d_{i,e}(T_e/\epsilon T_{ec})/dt \sim O(1)$, $\nabla(n/\epsilon n_c) \sim O(1)$ and $\nabla(T_e/\epsilon T_{ec}) \sim O(1)$.

It is also noted that we include the finite β effect in the reduced system to construct the energy conserving system. This procedure does not affect the dynamical contribution from ∇P_e. The energy conservation originally holds in the Braginskii's two-fluid equations, however it is occasionally lost in the reduced system during the reduction process.

Reduced two-fluid equations

The ordering and the derivation of the model equations are exactly the same as those in Ref.[23]. The shear Alfvén law is used to derive the vorticity equation. The parallel Ohm's law is derived by operating $(\mathbf{B}\cdot)$ to Eq.(39). $\nabla\cdot\mathbf{V}_e$ in Eq.(40) is calculated by using the electron velocity perpendicular to the magnetic field, which is estimated by Eq.(39) operated $(\mathbf{B}\times)$. Substituting ordered variables into these equations, the reduced set of equations is derived. As shown in the normalization, the ordering parameter is ϵ, and the reduced equations correspond to order-ϵ^2 components. In addition, our model equations including the neoclassical electron viscosity are derived by assuming cold ion and neglecting parallel ion momentum. The detailed derivation is given in Appendix.

Four-field reduced two-fluid equations $\{\phi$,A,n,$T\}$ are given by

$$\frac{D}{Dt}\nabla_\perp^2\phi = \nabla_\parallel j_\parallel + \mu\nabla_\perp^4\phi, \tag{38}$$

$$\frac{\partial}{\partial t}A = -\nabla_\parallel(\phi - \delta p) + \alpha_T\delta\nabla_\parallel T - \eta_\parallel\left(1+\sqrt{\epsilon}\right)j_\parallel + \eta_\parallel j_{\rm bs}, \tag{39}$$

$$\frac{D}{Dt}n + \beta\frac{D}{Dt}p = \beta\delta\nabla_\parallel j_\parallel + \beta\eta_\perp\nabla_\perp^2 p + \beta\mu^{\rm NC}\frac{1}{r}\frac{\partial}{\partial r}\left(rj_\parallel\right)$$
$$+ \beta\mu^{\rm NC}\frac{1}{r}\frac{\partial}{\partial r}\left(r\frac{\partial p}{\partial r}\right), \tag{40}$$

$$\frac{3}{2}\frac{D}{Dt}T - \frac{D}{Dt}n = \alpha_T\delta\beta\nabla_\parallel j_\parallel + \epsilon^2\chi_\parallel\nabla_\parallel^2 T + \chi_\perp\nabla_\perp^2 T, \tag{41}$$

where $(\hat{\mathbf{r}}, \hat{\boldsymbol{\theta}}, \hat{\mathbf{z}})$ indicate unit vectors. The plasma beta value is defined by $\beta = (4\pi/B_c^2)P_{ec}$. The ion skin depth normalized by the minor radius is $\delta = (1/a)(c/\omega_i)$, where $\omega_i = \sqrt{4\pi n_c e^2/m_i}$ is the ion plasma frequency. Eq.(38)-(41) are the vorticity equation, the generalized Ohm's law, the continuity equation, and the electron heat balance equation, respectively. In this study, parallel ion velocity is neglected. The variables $\{\phi, A, n, T, p\}$ indicate the electrostatic potential, the vector potential parallel to the ambient magnetic field, the electron density, the electron temperature and the pressure respectively. The electron pressure is approximated by $p = n + T$ in this model. The perturbed quantity f is assumed to vary as $f = f_0 + \tilde{f}$. Before normalization, the original pressure is given by $P_e = nT_e$, then the first order of the fluctuating part of pressure divided by P_{ec} is given by $\tilde{P}_e/P_{ec} = (\tilde{n}/n_c)(T_{e0}/T_{ec}) + (\tilde{T}_e/T_{ec})(n_0/n_c)$. In this formula, we approximate $n_0/n_c = 1$ and $T_0/T_c = 1$, therefore we simply define $p = n + T$ after normalization. It should be noted that these approximations are necessary not only for avoiding complicated terms caused by radial profiles, but also for constructing the energy conservation relation shown below. Let us note that this procedure qualitatively ensures the characteristics of gradient driven instability. Transport coefficients $\{\mu, \eta_\parallel, \eta_\perp, \chi_\parallel, \chi_\perp\}$ are the ion viscosity, the parallel resistivity, the perpendicular resistivity ($\eta_\perp\beta$ implies the particle diffusivity), the electron parallel thermal conductivity, and the electron perpendicular thermal conductivity, respectively.

In our model equations, neoclassical effects are included in Eq.(39) and Eq.(40), and electron viscosity is defined as

$$\mu^{\rm NC} = \eta_\parallel\frac{q}{\sqrt{\epsilon}}. \tag{42}$$

In our normalization, bootstrap current is defined by

$$j_{\rm bs} = -\frac{q}{\sqrt{\epsilon}}\frac{\partial p}{\partial r}. \tag{43}$$

which affects the stability of tearing mode by modifying the net electric current.

The energy conservation relation is written as

$$\frac{d}{dt}H = -\mu\int\left|\nabla_\perp^2\phi\right|^2 dV - \left(1+\sqrt{\epsilon}\right)\eta_\parallel\int\left|j_\parallel\right|^2 dV$$
$$- \eta_\perp\int\left|\nabla_\perp p\right|^2 dV - \frac{\epsilon^2\chi_\parallel}{\beta}\int\left|\nabla_\parallel T\right|^2 dV$$
$$- \frac{\chi_\parallel}{\beta}\int\left|\nabla_\perp T\right|^2 dV, \tag{44}$$

with

$$H = \frac{1}{2}\int |\nabla_\perp \phi|^2 dV + \frac{1}{2}\int |\nabla_\perp A|^2 dV + \frac{1}{2\beta}\int |n|^2 dV + \frac{3}{4\beta}\int |T|^2 dV + \frac{1}{2}\int |p|^2 dV, \quad (45)$$

where the integral indicates the volume integral over plasmas, and H is the Hamiltonian. In the dissipationless limit, this system conserves the energy[23,24]

4. Effects of neoclassical electron viscosity on drift-tearing mode

In this chapter, the linear stability and the nonlinear dynamics of the drift-tearing mode including neoclassical electron viscosity are investigated using the reduced two-fluid equations. Firstly, the effect of the neoclassical electron viscosity on the linear growth rate of the drift-tearing mode is examined by surveying parameter dependences. Analytical linear dispersion relation is derived to understand the physical mechanism. In the next step, the nonlinear evolution of magnetic island is simulated. The influence of the neoclassical electron viscosity on the saturated magnetic island width is examined.

4.1 Linear analysis

4.1.1 Analytical approach

In order to analyze the linear drift-tearing mode, a perturbed quantity $f(\mathbf{x},t)$ is assumed to vary as:

$$f_0(r) + \tilde{f}_{m,n}(r)\exp[im\theta + inz + (\gamma - i\omega_r)t], \quad (46)$$

in the cylindrical coordinates (Fourier expansion in θ and z directions), where m is a poloidal mode number and n is a toroidal mode number. $\{\gamma, \omega_r\}$ are the growth rate and the frequency of the mode, respectively. $\tilde{f}_{m,n}(r)$ satisfies the boundary conditions; $\tilde{f}_{m,n}(0) = 0$ and $\tilde{f}_{m,n}(1) = 0$.

The four-field model is linearized using the relations[23]:

$$\frac{D}{Dt}f \to \frac{\partial}{\partial t}\tilde{f}_{m,n} - ik_\theta f_0{}'\tilde{\phi}_{m,n},$$
$$\nabla_\parallel f \to ik_\parallel \tilde{f}_{m,n} + ik_\theta f_0{}'\tilde{A}_{m,n},$$
$$\nabla_\parallel^2 f \to -k_\parallel^2 \tilde{f}_{m,n} - k_\parallel k_\theta f_0{}'\tilde{A}_{m,n},$$
$$\nabla_\perp^2 f \to \left[\frac{1}{r}\frac{\partial}{\partial r}\left(r\frac{\partial}{\partial r}\right) - k_\theta^2\right]\tilde{f}_{m,n},$$

where the prime indicates the radial derivative and $k_\parallel = m/q(r) - n$, $k_\theta = m/r$ are parallel and perpendicular wave numbers, respectively. $q(r)$ is the safety factor defined by $1/q(r) = -(1/r)\partial A_0/\partial r$.

The linearized version of Eqs.(38)-(41) are written as:

$$-i\omega\nabla_\perp^2\tilde{\phi} = ik_\parallel\tilde{j}_\parallel + ik_\theta j_0'\tilde{A} + \mu\nabla_\perp^4\tilde{\phi}, \quad (47)$$

$$-i\omega\tilde{A} = -ik_\parallel\tilde{\phi} + i\delta k_\parallel\left[\tilde{n} + (1+\alpha_T)\tilde{T}\right] - i(\omega_{*n} + \omega_{*T})\tilde{A} - \eta_\parallel(1+\sqrt{\epsilon})\tilde{j}_\parallel - \mu^{\mathrm{NC}}\frac{\partial\tilde{p}}{\partial r}, \quad (48)$$

$$(1+\beta)\left(-i\omega\tilde{n} + i\frac{\omega_{*n}}{\delta}\tilde{\phi}\right) + \beta\left(-i\omega\tilde{T} + \frac{i}{1+\alpha_T}\frac{\omega_{*T}}{\delta}\tilde{\phi}\right) = \delta\beta\left(ik_\parallel\tilde{j}_\parallel + ik_\theta j_0'\tilde{A}\right) + \eta_\perp\beta\nabla_\perp^2\tilde{p} + \beta\mu^{\mathrm{NC}}\frac{1}{r}\frac{\partial}{\partial r}\left(r\tilde{j}_\parallel\right) + \beta\mu^{\mathrm{NC}}\frac{1}{r}\frac{\partial}{\partial r}\left(r\frac{\partial p}{\partial r}\right), \quad (49)$$

$$\frac{3}{2}\left(-i\omega\tilde{T} + \frac{i}{1+\alpha_T}\frac{\omega_{*T}}{\delta}\tilde{\phi}\right) - \left(-i\omega\tilde{n} + i\frac{\omega_{*n}}{\delta}\tilde{\phi}\right) = \alpha_T\delta\beta\left(ik_\parallel\tilde{j}_\parallel + ik_\theta j_0'\tilde{A}\right) - \epsilon^2\chi_\parallel\left(k_\parallel^2\tilde{T} - \frac{1}{1+\alpha_T}\frac{k_\parallel\omega_{*T}}{\delta}\tilde{A}\right) + \chi_\perp\nabla_\perp^2\tilde{T}, \quad (50)$$

where $\omega = \omega_r + i\gamma$ and we assume the relations: $\tilde{p} = \tilde{n} + \tilde{T}$ and $p_0'(r) = n_0'(r) + T_0'(r)$. For simplicity, the suffixes of mode numbers are omitted. $\{\omega_{*n}, \omega_{*T}\}$ are the diamagnetic drift frequency by the density and temperature gradient defined as:

$$\omega_{*n} = -\delta k_\theta n_0', \quad (51)$$
$$\omega_{*T} = -(1+\alpha_T)\delta k_\theta T_0'. \quad (52)$$

The equilibrium quantities are chosen as follows:

$$q(r) = q_0 + (q_r - q_0)\left(\frac{r}{r_s}\right)^3, \quad (53)$$
$$n_0'(r) = -\frac{2\beta_0}{\epsilon}r, \quad (54)$$
$$T_0'(r) = -\frac{2\beta_0}{\epsilon}r, \quad (55)$$

where $\beta_0 = \beta/(1-r_s^2)^2$ is β value at plasma center, and we set $\beta = 10^{-2}$, $\epsilon = 0.2, \mu = 10^{-5}$, $\eta_\perp = 2\times10^{-5}$, $\chi = 1$, $\eta_\parallel = \chi_\perp = 10^{-5}$, $r_s = 0.6$ as default values.

4.1.2 Analytical dispersion relation

Firstly, we derive the dispersion relation of the drift-tearing mode including the neoclassical effect. We employ the asymptotic matching method on the rational surface[25,26]. Far from the rational surface, solution is given by solving the ideal MHD equations. On the other hand, the resistivity (and other transport coefficients), the diamagnetic effects (and other kinetic effects) become important in the vicinity of the rational surface. In the following, these solutions are derived separately, and are matched in the overlapped region for deriving the dispersion relation.

Resistive MHD(Inner solution)

In order to derive inner layer equations, we assume $\nabla_\perp^2 \sim \partial^2/\partial x^2$ and $k_\parallel \sim k_\parallel' x$, where x is defined as

$x = r - r_s$ and r_s is the position of the rational surface. In addition, $j_0{}'$ term is neglected (this term is important for the kink mode but not for the tearing mode). Also, terms proportional to β in Eq.(49) and Eq.(50) are neglected. The transport coefficients except $\eta_\parallel$ and $\mu^{\rm NC}$ are set to zero for simplicity. For the nonlinear stability of the neoclassical tearing mode, the perturbation of temperature is important for the mode excitation. On the other hand, density and temperature play almost the same role for the mode, when the effect of thermal transport is not taken into account. For this reason, we use electron pressure p without distinguishing density and temperature, and diamagnetic drift frequency driven by electron pressure is defined by $\omega_* = -\delta k_\theta p_0'$. Then, equations in the inner layer are given by

$$-i\omega\phi'' = -ik_\parallel' xA'', \tag{56}$$

$$-i\omega A = -ik_\parallel' x\phi i + \delta\left(ik_\parallel' xp + ik_\theta p_0' A\right) + \left(1+\sqrt{\epsilon}\right)\eta_\parallel A'' - \mu^{\rm NC}\frac{\partial p}{\partial r}, \tag{57}$$

$$-i\omega p = ik_\theta p_0'\phi, \tag{58}$$

where the prime indicates the derivative $\partial/\partial x$, and tildes and suffixes are ignored for perturbed quantities, for simplicity. Substituting Eq.(58) into Eq.(57), equations are given by

$$-i\omega\phi'' = -ik_\parallel' xA'', \tag{59}$$

$$-i(\omega-\omega*)A = -\frac{ik_\parallel'}{\omega}x(\omega-\omega*)\phi + \eta_\parallel' A'' - \mu^{\rm NC}\frac{\omega_*}{\delta\omega}\frac{\partial\phi}{\partial x}, \tag{60}$$

where $\eta_\parallel' = (1+\sqrt{\epsilon})\eta_\parallel$. Fourier transforms of Eqs.(59)-(60) give

$$i\omega k^2\phi_k = -k_\parallel'\frac{dj_k}{dk}, \tag{61}$$

$$-i(\omega-\omega_*)\frac{j_k}{k^2} = k_\parallel'\frac{\omega-\omega_*}{\omega}\frac{d\phi_k}{dk} - \eta_\parallel' j_k + i\mu^{\rm NC}\frac{\omega_*}{\delta\omega}k\phi_k, \tag{62}$$

where

$$\phi_k = \int_{-\infty}^{\infty}\phi e^{-kx}dx,$$

$$A_k = \int_{-\infty}^{\infty}Ae^{-kx}dx,$$

$$j_k = -\int_{-\infty}^{\infty}A''e^{-kx}dx = k^2A_k.$$

By using Eqs.(61)-(62), we obtain

$$\frac{j_k}{k^2} = \frac{1}{\delta_{in}^2}\frac{d}{dk}\left(\frac{1}{k^2}\frac{dj_k}{dk}\right) - \delta_\eta^2 j_k + C_1\frac{dj_k}{dk}, \tag{63}$$

where $1/\delta_{in}^2 = -k_\parallel'^2/\omega^2$, $\delta_\eta^2 = i\eta_\parallel/\omega$ and $C_1 = ik_\parallel'\mu^{\rm NC}\omega_*/\delta\omega^2(\omega-\omega*)$. By setting $\sigma = \delta_{in}\delta_\eta k^2$, the equation becomes

$$\sigma\frac{d^2j_\sigma}{d\sigma^2} + \left(\sigma C_2 - \frac{1}{2}\right)\frac{dj_\sigma}{d\sigma} - \frac{1}{4}(\sigma+Q)j_\sigma = 0, \tag{64}$$

with $C_2 = C_1/2\cdot\delta_{in}/\delta_\eta$ and $Q = \delta_{in}/\delta\eta$. Considering a transformation $j_\sigma = e^{a\sigma}f$ and $\sigma = \xi Y$ with $a = -C_2 - \sqrt{C_2^2+1}/2$, $Y = \sigma/\xi$, we get

$$\xi\frac{\partial^2 f}{\partial\xi^2} + \frac{\partial f}{\partial\xi}(\gamma-\xi) - \alpha f = 0, \tag{65}$$

where $\gamma = -1/2$, $\alpha = Q - C_2 - \sqrt{C_2^2+1}/(4\sqrt{C_2^2+1})$. The solution of this equation is given by the confluent hypergeometric function such that

$$j_{\sigma,in} = j_1 e^{a\sigma}U\left(\alpha,\gamma,\beta^{-1}\sigma\right),$$

with

$$U\left(\alpha,\gamma,\beta^{-1}\sigma\right) = \frac{\pi}{\sin\pi\gamma}\{\frac{M\left(\alpha,\gamma,\beta^{-1}\sigma\right)}{\Gamma(1+\alpha-\gamma)} - \left(\beta^{-1}\sigma\right)^{1-\gamma}\frac{M\left(1+\alpha-\gamma,2-\gamma,\beta^{-1}\sigma\right)}{\Gamma(\alpha)\Gamma(2-\gamma)}\}, \tag{66}$$

where $M\left(\alpha,\gamma,\beta^{-1}\sigma\right)$ is confluent hyper geometric function of first kind defined as

$$M\left(\alpha,\gamma,\beta^{-1}\sigma\right) = \sum_{n=0}^{\infty}\frac{(\alpha)_n}{(\gamma)_n}\frac{z^n}{n!}. \tag{67}$$

Finally inner solution is given as

$$j_{\sigma,in} = j_1\left[\frac{\Gamma(3/2)}{\Gamma(\alpha+3/2)} + \frac{\Gamma(3/2)}{\Gamma(\alpha+3/2)}\left(-\frac{1}{2}\frac{\delta_{in}}{\delta_\eta}\right)\sigma + \frac{\Gamma(-3/2)}{\Gamma(\alpha)}\beta^{-3/2}\sigma^{3/2}\right] + O(\sigma^2). \tag{68}$$

Ideal MHD((Outer solution))

Equations in outer layer are given by

$$0 = -ik_\parallel A'' + ik_\theta j_0' A, \tag{69}$$

$$-i\omega A = -ik_\parallel\phi. \tag{70}$$

Considering Eq.(69), we model outer solution such that

$$A = A(0)\left(1 + \frac{\Delta'}{2}|x|\right), \tag{71}$$

where

$$\Delta' = \frac{A'(+0) - A'(-0)}{A(0)}.$$

Using Eq.(70), we obtain

$$\phi = \frac{\omega}{k_\parallel'}A(0)\left(\frac{1}{x} + \frac{\Delta'}{2}\frac{|x|}{x}\right). \tag{72}$$

where we approximate $k_\parallel \sim k_\parallel' x$. Fourier transform of Eq.(72) gives

$$\phi_{k,out}(k) = -\frac{i\omega}{k_\parallel'}A(0)\left\{\pi{\rm sgn}(k) + \frac{\Delta'}{k}\right\}, \tag{73}$$

where we use $\int_{-\infty}^{\infty}dx(1/x)e^{-ikx} = -i\pi{\rm sgn}(k)$ and $\int_{-\infty}^{\infty}dx\ {\rm sgn}(x)e^{-ikx} = -2i/k$. In order to match outer

solution Eq.(73) with inner solution Eq.(68), we assume that Fourier transform of current in the overlapped region is approximated by Eq.(73) transformed by Eq.(61) such that

$$j_{k,out} = -\frac{\omega^2}{k_\parallel'} A(0) \left\{ \frac{\pi}{3} k^3 \mathrm{sgn}(k) + \frac{\Delta'}{2} k^2 \right\} + C_0, \quad (74)$$

where C_0 is integral constant. Substituting Eq.(73) in Eq.(70), we obtain a boundary condition of $j_{k,out}$ in the limit of $k \to 0$.

$$j_{k,out} = -A(0)\Delta'. \quad (75)$$

Therefore, we obtain $C_0 = -A(0)\Delta'$. Finally inner solution is given as

$$j_{\sigma,out} = A(0) \left\{ \frac{\pi}{3} \frac{\delta_{in}^{1/2}}{\delta_\eta^{3/2}} \sigma^{3/2} + \frac{\Delta'}{2} \frac{\delta_{in}}{\delta_\eta} \sigma - \Delta' \right\}. \quad (76)$$

Matching of solutions

Matching in Eq.(68) with Eq.(76) (comparing coefficients), we obtain

$$\Delta' A(0) + \frac{\Gamma(3/2)}{\Gamma(\alpha + 3/2)} j_1 = 0, \quad (77)$$

$$\frac{\pi}{3} \frac{\delta_{in}^{1/2}}{\delta^{3/2}} A(0) - \frac{\Gamma(-3/2)}{\Gamma(\alpha)} \beta^{-3/2} j_1 = 0. \quad (78)$$

These equations have solutions $(A(0), j_1)$, when the following condition is satisfied.

$$-\Delta' \frac{\Gamma(-3/2)}{\Gamma(\alpha)} \beta^{3/2} - \frac{\Gamma(3/2)}{\Gamma(\alpha + 3/2)} \frac{\pi}{3} \frac{\delta_{in}^{1/2}}{\delta_\eta^{3/2}} = 0. \quad (79)$$

Using constant-ψ approximation[25], i.e. $\alpha = Q - C_2 - \sqrt{C_2^2 + 1}\sqrt{C_2^2 + 1} = Q/\sqrt{C_2^2+1} - C_2/\sqrt{C_2^2+1} - 1/4 \sim -C_2/\sqrt{C_2^2+1} - 1/4$, we obtain the dispersion relation as

$$\Delta' = -\frac{\pi}{8} \frac{\Gamma\left(-\frac{C_2}{\sqrt{C_2^2+1}} - 1/4\right)}{\Gamma\left(-\frac{C_2}{\sqrt{C_2^2+1}} + 5/4\right)} \frac{\delta_{in}^{1/2}}{\delta_\eta^{3/2}} \beta^{3/2}. \quad (80)$$

4.1.3 Analytical results

In the drift-tearing regime, $\omega_r \gg \gamma$, the linear growth rate derived from Eq.(80) is given such that

$$\gamma_{\mathrm{DT}} = \frac{1}{2} \left(\frac{1}{2\pi} \frac{\Gamma(1/4)}{\Gamma(3/4)} \right)^{4/3} k_\parallel'^{2/3} \omega_*^{-2/3} \eta_\parallel' \Delta'^{4/3}, \quad (81)$$

$$\gamma_{\mathrm{NDT}} = \left(\frac{1}{2\pi} \frac{\Gamma(1)}{\Gamma(1/2)} \right)^{2/3} \left(\mu^{\mathrm{NC}} \frac{\omega_*}{\delta} \right) k_\parallel'^{1/3} \omega_*^{-4/3} \Delta'^{2/3}, \quad (82)$$

where γ_{DT} corresponds to the growth rate of the pure drift-tearing mode case ($C_2 = 0$), and γ_{NDT} indicates the growth rate of the drift-tearing mode with the neoclassical electron viscosity ($C_2 \gg 1$). Note that γ_{NDT} is proportional to ω_*/δ, i.e. the pressure gradient, which is originally combined with the neoclassical electron viscosity as shown in the R.H.S. of Eq.(60). A ratio of Eq.(82) and Eq.(81) is

$$\frac{\gamma_{\mathrm{NDT}}}{\gamma_{\mathrm{DT}}} = \frac{\left(\frac{1}{2\pi} \frac{\Gamma(1)}{\Gamma(1/2)} \right)^{2/3}}{\left(\frac{1}{2\pi} \frac{\Gamma(1/4)}{\Gamma(3/4)} \right)^{4/3}} \left(\frac{\mu^{\mathrm{NC}}}{\eta_\parallel'} \frac{\omega_*}{\delta} \right) k_\parallel'^{-1/3} \omega_*^{-2/3} \Delta'^{-2/3} \gg 1, \quad (83)$$

in our parameters of interest. Therefore, it is found that the neoclassical effect destabilizes the drift-tearing mode. Because the neoclassical electron viscosity combines with the pressure gradient, this destabilization is originated by the free energy source of the pressure gradient.

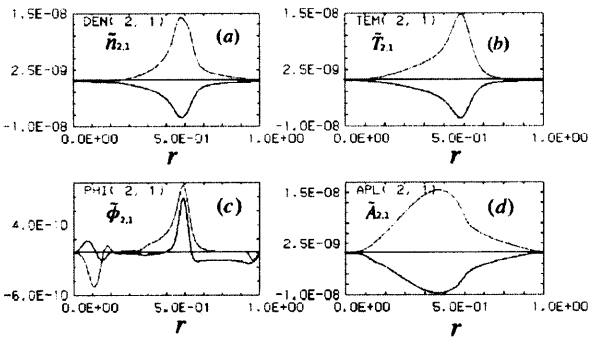

Fig. 4 Radial profiles of typical linear eigenfunctions of $(m, n) = (2, 1)$ mode; (a) density, (b) electron temperature, (c) scalar potential and (d) vector potential, respectively.

4.1.4 Numerical results

In the next step, we perform the linear stability analysis of the drift-tearing mode with the neoclassical electron viscosity, numerically.

Fig.4 shows the radial profiles of typical eigenfunctions $\{\tilde{\phi}, \tilde{A}, \tilde{n}, \tilde{T}\}$ of the (2,1) DTM. The vertical axis is arbitrary unit. The red and blue lines indicate the real and imaginary parts, respectively. In our model, Δ' can be controlled by changing the value of q_0.

Fig.5 shows the q_0 dependence of Δ' using safety factor profile Eq.(53), where $q_r = 2$, $r_s = 0.6$ are fixed. It is found that Δ' is a monotonic increasing function of q_0.

Fig.6 shows the dependence of the growth rate on Δ' with $\delta = 1.0 \times 10^{-2}$. Two cases are plotted: cases with and without the neoclassical electron viscosity. In the former case, the growth rate monotonically increases in the positive Δ' region, and becomes negative in the negative Δ' region, which agrees with the conventional drift-tearing mode theory. It is found that the drift-

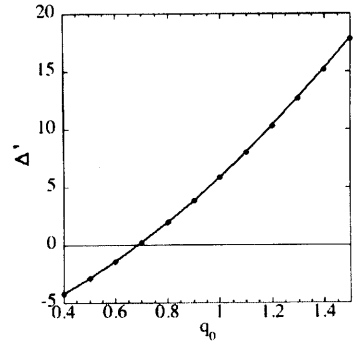

Fig. 5 Dependence of Δ' on q_0

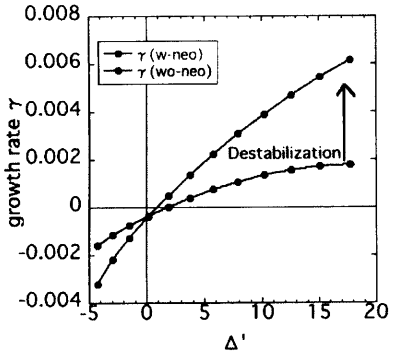

Fig. 6 Dependence of growth rate on Δ'

tearing mode is strongly destabilized by the neoclassical electron viscosity in the $\Delta' > 0$ regime. This result can be understood by the analytical dispersion relation derived in the previous subsection.

Fig.7 shows the dependence of the growth rate on δ with $\Delta' \sim 5$ ($q_0 = 1$), where electron diamagneic drift frequency is proportional to δ as shown in the definitions Eqs.(51)-(52). It is found that the pure drift-tearing mode is stabilized by the electron diamagnetic drift in the large δ region. The tendency of this result agree

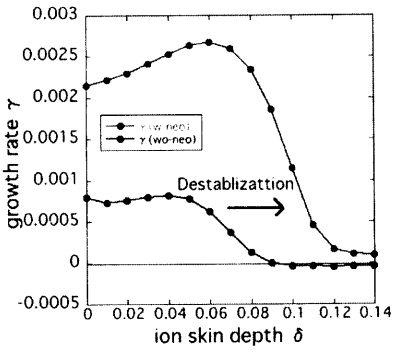

Fig. 7 Dependence of growth rate on δ

with analytical dispersion relation, which is monotonic decreasing functions of the electron diamagnetic drift frequency. The destabilizing in the small δ region is caused by the transport coefficients and terms neglected in the derivation of the dispersion relation. Similar to Fig.6, it is found that the drift-tearing mode is strongly destabilized by the neoclassical effect.

Thus, the analytical results given in the previous subsection is also confirmed by the numerical calculation. In conclusion, the neoclassical electron viscosity has a destabilizing effect on the linear drift-tearing mode.

4.2 Nonlinear analysis

In this section, nonlinear simulations of the drift-tearing mode are performed with or without neoclassical electron viscosity in the case with $\Delta' \sim 5$, where the drift-tearing mode is linearly unstable and its growth rate is enhanced by the neoclassical electron viscosity as confirmed in the previous section. We focus on the time evolution of magnetic island in the nonlinear regime and its nonlinear saturation width are discussed.

4.2.1 Analytical model of growth rate of magnetic island

Firstly, we derive the analytical decomposition of growth rate γ of vector potential which corresponds to the magnetic island so as to examine the saturation mechanism of the magnetic island, by using $(m,n) = (2,1)$ component of the Ohm's law and assuming $\tilde{A}_{2,1} \propto \exp(-i\omega t)$. The $(m,n) = (2,1)$ component of the Ohm's law is given by

$$\begin{aligned}\omega\tilde{A}_{2,1} &= (\omega_* + \tilde{\omega}_* + \tilde{\omega}_{E\times B})\tilde{A}_{2,1} \\ &+ k_{\parallel 2,1}\left[\tilde{\phi}_{2,1} - \delta\left\{\tilde{n}_{2,1} + (1+\alpha_T)\tilde{T}_{2,1}\right\}\right] \\ &+ i\eta_\parallel \nabla_\perp^2 \tilde{A}_{2,1} - i\mu^{\rm NC}\left(\frac{\partial\tilde{n}_{2,1}}{\partial r} + \frac{\partial\tilde{T}_{2,1}}{\partial r}\right) + N.L. \quad (84)\end{aligned}$$

with

$$\begin{aligned}\omega_* &= -\delta k_{\theta_{2,1}}[n_0' + (1+\alpha_T)T_0'], \\ \tilde{\omega}_* &= -\delta k_{\theta_{2,1}}[\tilde{n}_{0,0}' + (1+\alpha_T)\tilde{T}_{0,0}'], \\ \tilde{\omega}_{E\times B} &= k_{\theta_{2,1}}\tilde{\phi}_{0,0}', \\ k_{\theta_{2,1}} &= \frac{m}{r}, \\ k_{\parallel 2,1} &= m\left(\frac{1}{q} + \frac{1}{\tilde{q}}\right) - n, \\ \frac{1}{\tilde{q}} &= -\frac{1}{r}\tilde{A}_{0,0}',\end{aligned}$$

where the prime is the radial derivative and '*N.L.*' indicates nonlinear terms. Nonlinear terms are neglected, and they are important only when higher modes are dominant or unstable. In general the radial average over magnetic islands, each term in Eq.(84) is not constant inside magnetic islands; therefore, we take into account

to evaluate growth rate. Dividing Eq.(84) by $\tilde{A}_{2,1}$, radially averaging inside magnetic islands, and taking the imaginary part of ω, we obtain

$$\gamma = \mathrm{Im}\,(\omega) \approx \mathrm{Im}\left\langle L_{k_\parallel} \right\rangle + \mathrm{Im}\left\langle L_{\eta_\parallel} \right\rangle + \mathrm{Im}\,\langle L_{bs} \rangle\,, \quad (85)$$

with

$$L_{k_\parallel} = k_{\parallel 2,1} \frac{\tilde{\phi}_{2,1} - \delta\{\tilde{n}_{2,1} + (1+\alpha_T)\tilde{T}_{2,1}\}}{\tilde{A}_{2,1}},$$

$$L_{\eta_\parallel} = i\eta_\parallel \frac{\nabla_\perp^2 \tilde{A}_{2,1}}{\tilde{A}_{2,1}},$$

$$L_{\mathrm{bs}} = -i\mu^{\mathrm{NC}} \frac{1}{\tilde{A}_{2,1}} \left(\frac{\partial \tilde{n}_{2,1}}{\partial r} + \frac{\partial \tilde{T}_{2,1}}{\partial r} \right),$$

where $\langle\ \rangle$ means the radial average inside magnetic islands at each time step defined by

$$\langle\ \rangle = \frac{1}{W} \int_{r_{in}}^{r_{out}} dr, \quad (86)$$

with

$$W = r_{out} - r_{in}. \quad (87)$$

W, r_{in} and r_{out} are the width of magnetic island and radial positions of the inner and the outer separatrix, respectively. It should be noted that this operator implicitly depends on time via the position of the separatrix. we neglect nonlinear terms in Eq.(84) in the derivation of Eq.(85).

4.2.2 Numerical results

In the nonlinear simulation, $\delta = 10^{-2}$ and $q_0 = 1$ ($\Delta' \sim 5$) are used, and other transport coefficients and equilibrium profiles are the same as those in the linear analysis. Only $(m,n) = (2,1),(0,0)$ are included for simplicity. We confirmed that the nonlinear evolution and saturation width of magnetic island is slightly affected by higher modes.

Figs.8 and 9 show the time evolutions of energies defined by $E_\phi = 1/2 \cdot |\nabla_\perp \phi_{m,n}|^2$, $E_A = 1/2 \cdot |\nabla_\perp A_{m,n}|^2$, $E_n = 1/2\beta \cdot |\nabla_\perp n_{m,n}|^2$, $E_T = 3/4\beta |\nabla_\perp T_{m,n}|^2$, respectively. The cases with (Fig.8) and without (Fig.9) the neoclassical electron viscosity are shown. In comparison with two cases, the linear growth of modes in the former case is much faster than the latter, due to the enhancement by neoclassical electron viscosity. Note that, in the former case, energy of $(m,n) = (2,1)$ decreases after the first peak, and saturates in the lower energy level. This kind of behavior is not observed in the latter case, therefore it is due to neoclassical electron viscosity.

Figs.10 and 11 show the radial profiles of equilibrium density and temperature at $t = 0$ (initial profile) and 25000 (nonlinear saturation state) in the case with or without neoclassical electron viscosity. It is found that the equilibrium density is modified in the range from

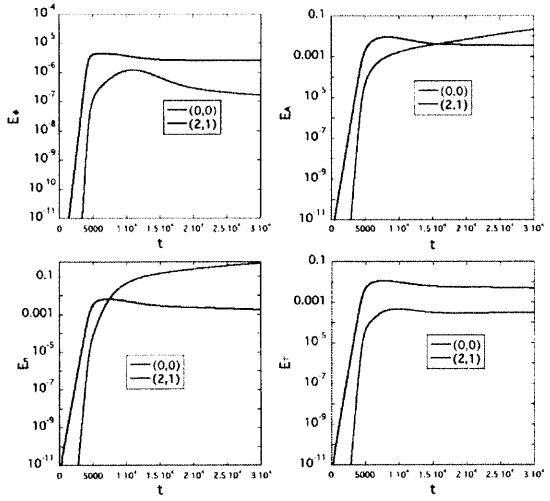

Fig. 8 The time evolutions of energy in the case with the neoclassical electron viscosity

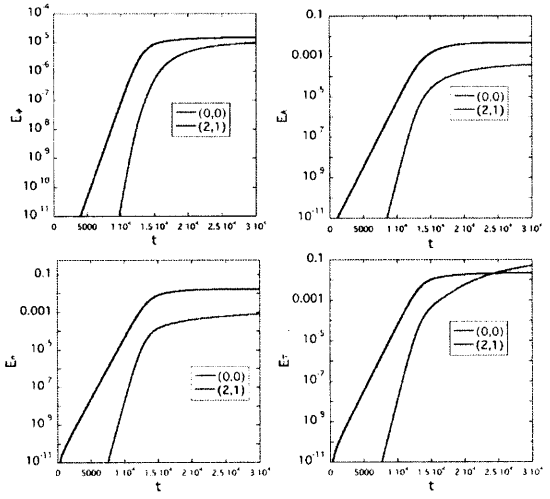

Fig. 9 The time evolutions of energy in the case without the neoclassical electron viscosity

center to magnetic island region. While, the equilibrium temperature is slightly changed. This difference between equilibrium density and temperature is caused by the diffusion via neoclassical electron viscosity, which is associated with the third and fourth terms in R.H.S. of Eq.(40). The strong diffusion in the center region is due to the factor $(1/r)$ in these terms. In general, magnetic island tends to flatten equilibrium pressure gradient inside magnetic island separatrix. However, this flattening is not strong as shown in Fig.11, when the width of magnetic island is small. In the case without neoclassical electron viscosity, the equilibrium density is not strongly affected by the magnetic island, but the equilibrium temperature is weakly affected.

Fig.12 shows the time evolution of the magnetic is-

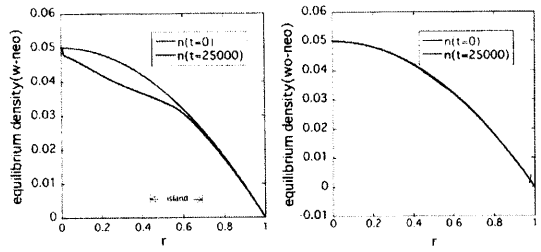

Fig. 10 The radial profiles of the density at t = 0, 25000

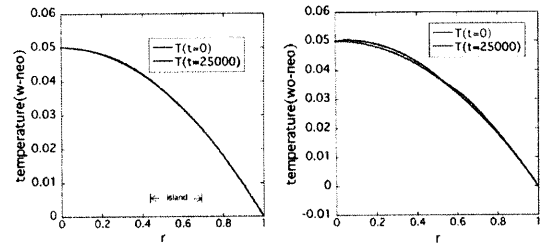

Fig. 11 The radial profiles of the temperature at t = 0, 25000

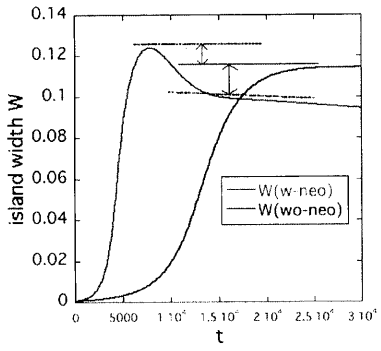

Fig. 12 The time evolutions of the magnetic island width.

land width. Two cases are plotted; cases with (w-neo) and without (wo-neo) neoclassical electron viscosity, respectively. In the early stage, the linear growth in the former case is faster than the latter, which is similar to those in Fig.8 and Fig.9. In contrast with the enhancement of the linear growth, the saturation level is weakly affected by neoclassical electron viscosity. In addition, it is remarkable that the saturation width of magnetic island in the former case temporally overcomes the latter($t = 5000$), however final saturation width becomes lower.

Figs.13 and 14 show the time evolution of growth rate and rotation frequency of magnetic island. Two cases are plotted; cases with (w-neo) and without (wo-neo) neoclassical electron viscosity, respectively. In the former case, corresponding to the Fig.12, the negative

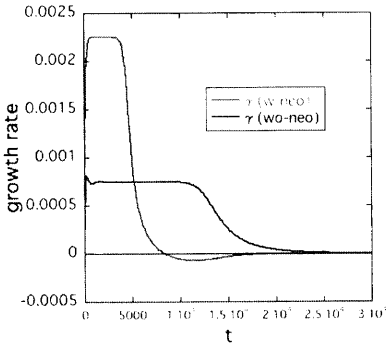

Fig. 13 The time evolutions of the growth rate γ.

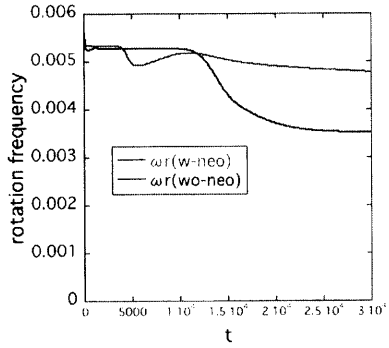

Fig. 14 The time evolutions of the rotation frequency ω_r.

growth rate is observed in the transient phase. The time evolution of rotation frequency is mainly dominated by $E \times B$ flow and electron diamagnetic flow, which are nonlinearly excited and modified by magnetic island. In this study, the influence of neoclassical electron viscosity on the rotation frequency is not investigated in detail. It should be investigated as a future work.

The interpretation of behavior of magnetic island in Fig.12 is not straightforward from a view point of the standard modified Rutherford model, i.e. one expects that the saturation width of magnetic island might be enhanced by neoclassical electron viscosity. In order to clarify the saturation mechanism of magnetic island in the presence of neoclassical electron viscosity, the growth rate of magnetic island is decomposed into each component by using the analytical model of growth rate derived in the previous subsection, Eq.(85).

Figs.15 and 16 show time evolution of growth rate and components in Eq.(85) in cases with (w-neo) and without (wo-neo) neoclassical electron viscosity. 'γ' indicates the growth rate, and '$L_{k_\parallel}$', '$L_{\eta_\parallel}$' and '$L_{\rm bs}$' correspond to the first, the second and the third terms in Eq.(85). The summation of them approximately reconstructs the growth rate. In Fig.15, it is found that '$L_{k_\parallel}$' is not effective in the saturation phase, and the

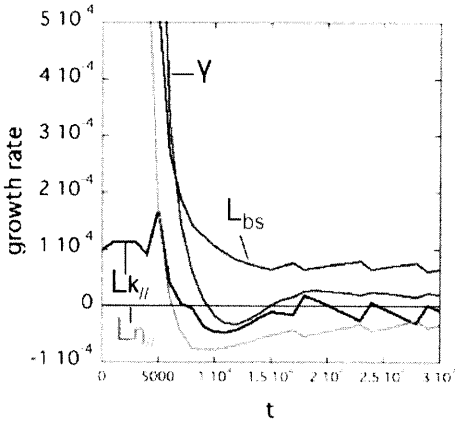

Fig. 15 The time evolution of each component of growth rate in the case with the neoclassical electron viscosity.

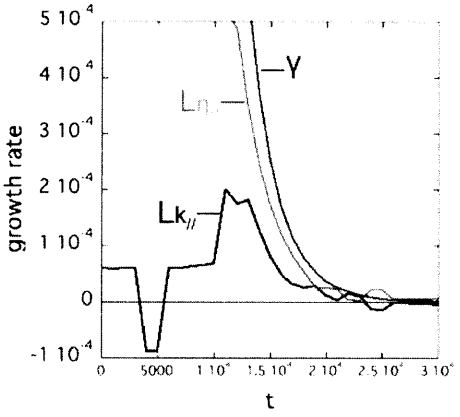

Fig. 16 The time evolution of each component of growth rate in the case without the neoclassical electron viscosity.

dynamics is mainly dominated by '$L_{\eta_\parallel}$' and 'L_{bs}', in other words, the saturation width is mainly determined by the balance of '$L_{\eta_\parallel}$' and '$L_{\rm bs}$', where $L_{\rm bs}$ implies the contribution from neoclassical electron viscosity. The nonlinear term which is neglected in the analytic model might play a role for complete cancellation. Here '$L_{\eta_\parallel}$' is associated with nonlinearly modified Δ' such that

$$\begin{aligned}\mathrm{Im}\left\langle L_{\eta_\parallel}\right\rangle &= \mathrm{Im}\left\langle i\eta_\parallel \frac{\nabla_\perp^2 \tilde{A}_{2,1}}{\tilde{A}_{2,1}}\right\rangle \\ &\sim \frac{\eta_\parallel}{W}\mathrm{Im}\left\{ i\frac{\tilde{A}'_{2,1}(r_{out}) - \tilde{A}'_{2,1}(r_{in})}{\tilde{A}_{2,1}(r_s)}\right\} \\ &\sim \frac{\eta_\parallel}{W}\Delta' \end{aligned} \tag{88}$$

where Δ' is nonlinearly modified one. Therefore, nonlinear evolution of Δ' should be examined in detail.

Fig.17 shows time evolution of Δ' in cases with (w-neo) and without (wo-neo) neoclassical electron viscosity, respectively. Δ' is estimated by

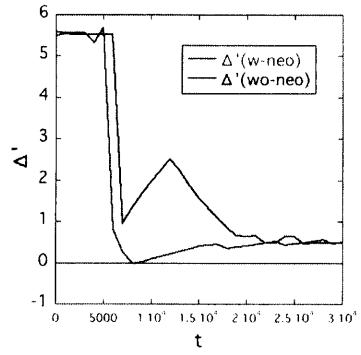

Fig. 17 The time evolutions of Δ'

$$\Delta' = \mathrm{Re}\left\{ \frac{\tilde{A}'_{2,1}(r_{out}) - \tilde{A}'_{2,1}(r_{in})}{\tilde{A}_{2,1}(r_s)}\right\}. \tag{89}$$

In the linear regime, r_{out} and r_{in} are given by width of linear boundary layer. In this study, the width of boundary layer is determined such as it can produce the initial Δ'. When magnetic island width overcomes the boundary layer width, r_{out} and r_{in} are replaced by the positions of outer and inner separatrixes. The small peak observed in the pure drift-tearing mode case, from $t = 6000$ to $t = 12000$, is caused by the error in the estimation of Δ' in the transient phase from linear regime to nonlinear regime, and which is not essential. It is found that Δ' in the saturation regime in the pure drift-tearing mode case is small but finite. On the other hand, '$L_{\eta_\parallel}$' in Fig.16 converges to zero. This implies that the approximation from the first line to the second line in Eq.(88) is not accurate, due to the failure of the so-called constant ψ approximation. Thus, '$L_{\eta_\parallel}$' could be negative even when Δ' is positive. In comparison with two cases in Fig.17, Δ' becomes lower via neoclassical electron viscosity, which makes '$L_{\eta_\parallel}$' negative.

In conclusion, the saturation width of magnetic island is affected by neoclassical electron viscosity via two channels: one is the direct enhancement of growth by bootstrap current, and the other is the indirect effect on Δ', which is not taken into account in the standard modified Rutherford theory. In this thesis, the effects of neoclassical electron viscosity on the drift-tearing mode have been investigated by numerical simulations and analytical calculations based on the reduced set of two-fluid equations.

In Chapter 4, the linear and nonlinear analyses of the drift-tearing mode is performed.

(1)The dispersion relation of the drift-tearing mode including the neoclassical electron viscosity effect is derived. The asymptotic matching method on the rational surface is employed. As a result, it is found that the

neoclassical effect contributes to the destabilization of the drift-tearing mode. The pressure gradient becomes a free energy source of the instability through the neoclassical electron viscosity.

(2)The linear stability analysis of the drift-tearing mode with the neoclassical electron viscosity is done, numerically. The dependence of the growth rate on each parameter is investigated. It is found that the drift-tearing mode is strongly destabilized by the neoclassical electron viscosity for $\Delta' > 0$. This result can be understood by the analytical dispersion relation. We confirm that the drift-tearing mode is stabilized by the drift parameter δ, which is reported by old DTM papers.

(3)The nonlinear behavior of the drift-tearing mode with or without neoclassical electron viscosity is also examined for the case with $\Delta' \sim 5$, where the drift-tearing mode is linearly unstable and its growth rate is enhanced by the neoclassical electron viscosity. We have derived the analytical decomposition of growth rate γ of vector potential which corresponds to the magnetic island so as to examine the saturation mechanism of the magnetic island. In the nonlinear simulations, $\delta = 10^{-2}$ is used, and other transport coefficients and equilibrium profiles are the same as those in the linear analysis. Only $(m,n) = (2,1),(0,0)$ are included for simplicity. The time evolutions of energies with and without the neoclassical electron viscosity are shown. For the former case, it is found that the energy of $(m,n) = (2,1)$ decreases after the first peak, and saturates in the lower energy level. This kind of behavior is not observed for the latter case, therefore it is concluded that it comes from the neoclassical electron viscosity. The radial profiles of equilibrium density and temperature are compared in the initial and nonlinear saturation phases. It is found that the profile of the density is greatly modified. In the case without neoclassical electron viscosity, the equilibrium density is not strongly affected by the magnetic island, but the equilibrium temperature is weakly affected. In contrast with the enhancement of the linear growth, the saturation level of magnetic island is weakly affected by neoclassical electron viscosity. In addition, it is remarkable that the saturation width of magnetic island in the former case temporally overcomes the latter, however final saturation width becomes smaller. In the time evolution of the magnetic island width, the negative growth rate is observed in the transient phase. It is shown that $L_{k_\parallel}$ is not effective in the saturation phase, and the dynamics is mainly dominated by $L_{\eta_\parallel}$ and $L_{\rm bs}$, in other words, the saturation width is mainly determined by the balance of $L_{\eta_\parallel}$ and $L_{\rm bs}$, where $L_{\rm bs}$ implies the contribution from neoclassical electron viscosity. We also evaluated Δ' assuming constant Ψ approximation, it is found that Δ' in the saturation phase is small but finite for the pure drift-tearing mode. On the other hand, $L_{\eta_\parallel}$ converges to zero. It is found that constant Ψ approximation is broken and the sign of $L_{\eta_\parallel}$ is not corresponding to that of Δ'.

Acknowledgements

This work is partially supported by Grant-in-Aid for Specially-promoted Research (16002005), by Grant-in-Aid for Scientific Research B (19360415) and by collaboration program of the Research Institute for Applied Mechanics of Kyushu University.

References

1) J. Wesson. *Tokamaks (second edition)*, Oxford Science Publications (1997).
2) ITER Physics Basis Editors, ITER Physics Expert Group Chairs and Co-Chairs and ITER Joint Central Team and Physics Integration Unit. Nuclear Fusion **39** (1999) 2137.
3) Y. Ishii and T. Ozeki and S. Tokuda and T. Fujita and Y. Kamada and S. Ishida and S Takeji. Plasma Phys. Control. Fusion **40** (1998) 1607.
4) H. Zohm and G. Gantenbein and A. Isayama and A. Keller and R. J. La Haye and M. Maraschek and A. Mück and K. Nagasaki and S. D. Pinches and E. J. Strait. Plasma Phys. Control. Fusion **45** (2003) 163.
5) R. J. La Haye. Phys. Plasmas **13** (2006) 055501.
6) S. -I. Itoh and K. Itoh and H. Zushi and A. Fukuyama. Plasma Phys. Control. Fusion **40** (1998) 879.
7) M. Maraschek and G. Gantenbein and T. P. Goodman and S. Günter and D.F. Howell and F. Leuterer and A. Mück and O. Sauter and H. Zohm and Contributors to the EFDA-JET Workprogrammea and the ASDEX Upgrade Team. Nucl. Fusion **45** (2005) 1369.
8) R. Fitzpatrick, and F. L. Waelbroeck. Phys. Plasmas **15** (2008) 012502.
9) A. I. Smolyakov. Plasma Phys. Control. Fusion **35** (1993) 657.
10) P. H. Diamond and S. -I. Itoh and K. Itoh and and T. S. Hahm", year = "Plasma Phys. Control. Fusion **47** (2005) R35.
11) M. F. F. Nave and J. A. Wesson. Nucl. Fusion **30** (1990) 2575.
12) Nishimura Seiya. Phys. Plasmas **15** (2008) 092506-092506-10.
13) P.H Diamond and R. D. Hazeltine and Z. G. An and B. A. Carreras and H. R. Hicks. Phys. Fluids **27** (1984) 1449.
14) A. Bierwage and S. Hamaguchi and M. Wakatani

and S. Benkadda and X. Leoncini. Phys. Rev. Lett. **94** (2005) 065001.
15) R. J. La Haye and L. L. Lao and E. J. Strait and T. S. Taylor. Nucl. Fusion **37** (1997) 397.
16) P. H. Rutherford. Phys. Fluids **16** (1973) 1903.
17) H. P. Furth and J. Killeen and M. N. Rosenbluth. Phys. Fluids **6** (1963) 459.
18) J. F. Drake and Y. C. Lee. Phys. Fluids **20** (1977) 1341.
19) J. F. Drake and T. M. Antonsen Jr. and A. B. Hassam and N. T. Gladd. Phys. Fluids **26** (1983) 2509.
20) R. B. White and D. A. Monticello. Phys. Fluids **20** (1977) 800.
21) B. D. Scott and A. B. Hassam. Phys. Fluids **30** (1987) 90.
22) J. D. Callen and W. X. Qu and others. Proc. 11th Int. Conf. Plasma Physics and Controlled Nuclear Fusion Research, Kyoto **2** (1987) 149.
23) R. D. Hazeltine and J. D. Meiss. Phys. Rep. **121** (1985) 1.
24) C. T. Hsu and R. D. Hazeltine and P. J. Morrison. Phys. Fluids **29** (1986) 1480.
25) S. Migliuolo and F. Pegoraro and F. Porcelli. Phys. Fluids B **3** (1991) 1338.
26) G. Ara and B. Basu and B. Coppi and G. Laval and M. N. Rosenbluth and B. V. Waddell. Ann. Phys. (NY) **112** (1978) 443.

Appendix

A1. Derivation of equations

A1.1 Kinetic equations

The fundamental equations describing dynamics of high temperature plasmas confined by magnetic fields are the Boltzmann equation (Vlasov equation with the collision term, $C(f_s, f_s)$) and Maxwell equations:

$$\frac{\partial f_s}{\partial t} + \mathbf{v}_s \cdot \nabla f_s + \frac{q_s}{m_s}\left(\mathbf{E} + \frac{1}{c}\mathbf{v}_s \times \mathbf{B}\right) \cdot \frac{\partial f_s}{\partial \mathbf{v}_s} = C(f_s, f_s) \tag{A1}$$

$$\nabla \cdot \mathbf{E} = 4\pi \sum_s q_s \int f_s d^3 v_s \tag{A2}$$

$$\nabla \cdot \mathbf{B} = 0 \tag{A3}$$

$$\frac{1}{c}\frac{\partial}{\partial t}\mathbf{E} = -\frac{4\pi}{c}\sum_s q_s \int \mathbf{v}_s f_s d^3 v_s \tag{A4}$$

$$\frac{1}{c}\frac{\partial}{\partial t} = -\nabla \times \mathbf{E} \tag{A5}$$

where $f_s = f_s(\mathbf{x}, \mathbf{v}_s, t)$ is the number of particles at the point $\mathbf{x}$ with velocity $\mathbf{v}_s$ at time t. cgs units are used and the suffix s denotes a species of the charged particle. q_s and m_s are the mass and the electric charge of species-s particles, respectively. c is the velocity of light. $\mathbf{E}(\mathbf{x}, t)$ and $\mathbf{B}(\mathbf{x}, t)$ are electric field and magnetic field, respectively. For inhomogeneous magnetically confined plasmas, it is not easy to apply the Boltzmann equation to them directly. When macroscopic behaviors or long wavelength fluctuations are important, fluid equations derived from the Boltzmann equation are used.

A1.2 Braginskii's equations

By operating $\int dv_s^3\ \mathbf{v}_s^n$ $(n = 0, 1, 2, ...)$ on Boltzmann equations, fluid equations are derived. Equations for $n = 0, 1, 2$ moments describe the time evolutions of density, momentum and pressure. This set of equations is called transport equations, where appropriate closures are necessary for applications. One of the most successful model is the Braginskii's two-fluid equations, which consist of the continuity equation, the momentum equation and the heat balance equation for the electrons and for the ions:

$$\frac{d_i}{dt} n_i + n_i \nabla \cdot \mathbf{V}_i = 0, \tag{A6}$$

$$\frac{d_e}{dt} n_e + n_e \nabla \cdot \mathbf{V}_e = 0, \tag{A7}$$

$$m_i n_i \frac{d_i \mathbf{V}_i}{dt} = -\nabla P_i - \nabla \cdot \pi_i + e n_i \left(\mathbf{E} + \frac{1}{c}\mathbf{V}_i \times \mathbf{B}\right) + \mathbf{R}_{ei}, \tag{A8}$$

$$m_e n_e \frac{d_e \mathbf{V}_e}{dt} = -\nabla P_e - \nabla \cdot \pi_e - e n_e \left(\mathbf{E} + \frac{1}{c}\mathbf{V}_e \times \mathbf{B}\right) + \mathbf{R}_{ie}, \tag{A9}$$

$$\frac{3}{2} n_i \frac{d_i}{dt} T_i + P_i \nabla \cdot \mathbf{V}_i = \nabla \cdot \mathbf{q}_i - \pi_i : \nabla \mathbf{V}_i + Q_i, \tag{A10}$$

$$\frac{3}{2} n_e \frac{d_e}{dt} T_e + P_e \nabla \cdot \mathbf{V}_e = \nabla \cdot \mathbf{q}_e - \pi_e : \nabla \mathbf{V}_e + Q_e, \tag{A11}$$

with closures

$$\begin{aligned}\frac{1}{en}\mathbf{R}_{ie} =&\eta_{\parallel}\mathbf{J}_{\parallel}+\eta_{\perp}\mathbf{J}_{\perp}-\frac{\alpha_T}{e}\mathbf{b}\left(\mathbf{b}\cdot\nabla\right)T,\\ \mathbf{q}_i =&-\kappa_{\parallel i}\mathbf{b}\cdot\nabla T_i-\kappa_{\perp i}\left(\nabla-\mathbf{b}\left(\mathbf{b}\cdot\nabla\right)\right)T_i\\ &+\frac{5}{2}\frac{cn_iT_i}{eB}\mathbf{b}\times\nabla T_i-\frac{\alpha_T}{e}T_i\mathbf{J}_{\parallel},\\ \mathbf{q}_e =&-\kappa_{\parallel e}\mathbf{b}\cdot\nabla T_e-\kappa_{\perp e}\left(\nabla-\mathbf{b}\left(\mathbf{b}\cdot\nabla\right)\right)T_e\\ &+\frac{5}{2}\frac{cn_eT_e}{eB}\mathbf{b}\times\nabla T_e-\frac{\alpha_T}{e}T_e\mathbf{J}_{\parallel},\end{aligned}$$

where $\mathbf{V}_{i,e}$ is the fluid velocity, $n_{i,e}$ is the density, $P_{i,e}=n_{i,e}T_{i,e}$ is the isotropic pressure, $\pi_{i,e}$ is the anisotropic stress tensor, $T_{i,e}$ is the temperature, $\mathbf{q}_{i,e}$ is the heat flux and $Q_{i,e}$ is the heat source, where the suffix i,e indicates ions or electrons, respectively . In this study, Hydrogen plasmas are considered for simplicity. e is the electric charge and a numerical factor $\alpha_T=0.71$ for Hydrogen plasmas. Momentum exchange terms $\mathbf{R}_{ei}$ and $\mathbf{R}_{ie}$ satisfy $\mathbf{R}_{ei}+\mathbf{R}_{ie}=0$. The time derivatives are defined $d_i/dt=\partial/\partial t+\mathbf{V}_i\cdot\nabla$ and $d_e/dt=\partial/\partial t+\mathbf{V}_e\cdot\nabla$. Magnetic field is $\mathbf{B}=B\mathbf{b}$, where $\mathbf{b}$ is an unit vector along the magnetic field line. Electric current is $\mathbf{J}=(4\pi/c)\nabla\times\mathbf{B}$, and $\mathbf{J}_{\parallel}$ and $\mathbf{J}_{\perp}$ are electric current parallel and perpendicular to magnetic field lines. Transport coefficients $\{\eta_{\parallel},\eta_{\perp},\kappa_{\parallel i},\kappa_{\perp i},\kappa_{\parallel e},\kappa_{\perp e}\}$ are parallel resistivity, perpendicular resistivity, parallel ion heat conductivity, perpendicular ion heat conductivity, parallel electron heat conductivity and perpendicular electron heat conductivity, respectively.

A1.3 Derivation of shear Alfvén law

Firstly, magnetic field curvature is introduced as $\boldsymbol{\kappa}=(\mathbf{b}\cdot\nabla)\mathbf{b}$. Then, the curvature is transformed such that $\boldsymbol{\kappa}=-\mathbf{b}\times(\nabla\times\mathbf{b})=\mathbf{b}\times(\nabla\times\mathbf{B})/B-\nabla_{\perp}B/B=(4\pi/c)\mathbf{J}\times\mathbf{B}/B^2+\nabla_{\perp}B/B$, where $(\mathbf{b}\cdot\nabla)\mathbf{b}=(1/2)\nabla b^2-\mathbf{b}\times(\nabla\times\mathbf{b})=-\mathbf{b}\times(\nabla\times\mathbf{b})$ and $\nabla_{\perp}=\nabla-\mathbf{b}(\mathbf{b}\cdot\nabla)$ are used. If $\mathbf{f}=m_in(d\mathbf{V}/dt)+\nabla\cdot\pi_i$ is defined, we obtain $\boldsymbol{\kappa}=(4\pi/c)\mathbf{J}\times\mathbf{B}/B^2+\nabla_{\perp}B/B=(4\pi/B^2)(\mathbf{f}+\nabla P_e)+(\nabla_{\perp}B/B)$. By operating $(\mathbf{B}\cdot\nabla\times)$ to Eq.(31), $c\mathbf{B}\cdot\nabla\times\mathbf{f}=\mathbf{B}\cdot\nabla\times(\mathbf{J}\times\mathbf{B})$ is obtained. The right hand side of this equation is $\mathbf{B}\cdot\nabla\times(\mathbf{J}\times\mathbf{B})=-\nabla\cdot(B^2\mathbf{J}_{\perp})=B^2\mathbf{B}\cdot\nabla(J_{\parallel}/B)-(1/B^2)\mathbf{B}\times(\mathbf{J}\times\mathbf{B})\cdot\nabla_{\perp}B^2=B^2\mathbf{B}\cdot\nabla\left(J_{\parallel}/B\right)-(c/4\pi)\mathbf{B}\times\boldsymbol{\kappa}\cdot\nabla_{\perp}B^2$, where $\mathbf{J}=\mathbf{J}_{\perp}+J_{\parallel}\mathbf{b}$, $\mathbf{J}_{\perp}=\mathbf{B}\times(\mathbf{J}\times\mathbf{B})/B^2$, $\nabla\cdot\mathbf{J}=\nabla\cdot\mathbf{J}_{\perp}+\mathbf{B}\cdot\nabla(J_{\parallel}/B)=0$ and $\boldsymbol{\kappa}=(4\pi/c)\mathbf{J}\times\mathbf{B}/B^2+\nabla_{\perp}B/B$ are used. Then, we get the shear Alfvén law as

$$c\mathbf{B}\cdot\nabla\times\mathbf{f}=B^2\mathbf{B}\cdot\nabla\left(\frac{J_{\parallel}}{B}\right)-\frac{c}{4\pi}\mathbf{B}\times\boldsymbol{\kappa}\cdot\nabla_{\perp}B^2. \tag{A12}$$

Substituting $\boldsymbol{\kappa}=(4\pi/B^2)(\mathbf{f}+\nabla P_e)+\nabla_{\perp}B/B$ to eliminate $\nabla_{\perp}B^2$, we get an alternative form as

$$\begin{aligned}c\mathbf{B}\cdot(\nabla\times\mathbf{f}-2\boldsymbol{\kappa}\times\mathbf{f})=&B^2\mathbf{B}\cdot\nabla\left(\frac{J_{\parallel}}{B}\right)+2c\mathbf{B}\\ &\times\boldsymbol{\kappa}\cdot\nabla_{\perp}P_e.\end{aligned} \tag{A13}$$

A1.4 Derivative of unit vectors

In our coordinate introduced in section 3., unit vectors satisfy the following relations: $\partial\hat{\mathbf{x}}/\partial z=\hat{\mathbf{z}}$, $\partial\hat{\mathbf{z}}/\partial z=-\hat{\mathbf{x}}$, $\partial\hat{\mathbf{z}}/\partial x=0$ and $\partial\hat{\mathbf{z}}/\partial y=0$, which are derived from $\partial\hat{\mathbf{R}}/\partial\zeta=\hat{\boldsymbol{\zeta}}$, $\partial\hat{\boldsymbol{\zeta}}/\partial\zeta=-\hat{\mathbf{R}}$, $\partial\hat{\boldsymbol{\zeta}}/\partial R=0$ and $\partial\hat{\boldsymbol{\zeta}}/\partial Z=0$.

A1.5 Derivation of reduced set

We apply approximations as $n/n_c=1$ and $T_e/T_{ec}=1$ in some steps during the following reduction process. This approximation may be inconsistent, because the radial profile effects of n and T_e are not kept strictly, and it cannot be justified by the present ordering process. However, it reduces the complexity of the system (especially avoiding the cubic nonlinearity) and provides the simple description for gradients of density and temperature, which contribute to the dynamics of the instability and the rotation. This procedure is similar to so-called Boussinesq approximation in the neutral fluid dynamics.

Firstly, the reduced shear-Alfvén law is derived. Normalized form of Eq.(31) is written as

$$\epsilon^2\frac{n}{n_c}\frac{d_i\mathbf{u}}{dt}=-\epsilon\nabla p+\epsilon^2\nabla\cdot\pi_i+(\nabla\times\mathbf{B})\times\mathbf{B} \tag{A14}$$

Then normalized shear Alfvén law Eq.(35) is given by

$$\begin{aligned}&\epsilon^2\mathbf{B}\cdot(\nabla-2\boldsymbol{\kappa})\times\left(\frac{n}{n_c}\frac{d_i\mathbf{u}}{dt}+\nabla\cdot\pi_i\right)\\ &=B^2\mathbf{B}\cdot\nabla\left(\frac{J_{\parallel}}{B}\right)+2\epsilon\mathbf{B}\times\boldsymbol{\kappa}\cdot\nabla_{\perp}p,\end{aligned} \tag{A15}$$

where $d_i/dt=\partial/\partial t+\mathbf{u}\cdot\nabla$. We gather $O(\epsilon^2)$ components in Eq.(A15), which describe the shear-Alfvén dynamics. Components corresponding to the compressional Alfvén dynamics are less than $O(\epsilon^3)$. Magnetic field and current are $\mathbf{B}=\hat{z}+\epsilon(-\hat{z}x+\hat{z}B_{\parallel}-\hat{z}\times\nabla_{\perp}A)+\mathrm{O}(\epsilon^2)$ and $\mathbf{J}=\nabla\times\mathbf{B}=\epsilon(\nabla_{\perp}B_{\parallel}\times\hat{\mathbf{z}}-\hat{\mathbf{z}}\nabla_{\perp}^2A)+O(\epsilon^2)$. Normalized curvature is $\boldsymbol{\kappa}=(4\pi/B^2)(\mathbf{f}+\nabla P)+\nabla_{\perp}B/B\rightarrow\epsilon\nabla_{\perp}\left(p+B_{\parallel}-x\right)+O(\epsilon^2)=-\epsilon\nabla_{\perp}x+O(\epsilon^2)\sim O(\epsilon)$, where $\mathbf{f}\sim O(\epsilon^2)$ and $B^2=1+2\epsilon(-x+B_{\parallel})+O(\epsilon)$ and a relation $\epsilon(\nabla_{\perp}B_{\parallel}+\nabla_{\perp}p)\sim O(\epsilon^2)$ is used. The relation $\epsilon(\nabla_{\perp}B_{\parallel}+\nabla_{\perp}p)\sim O(\epsilon^2)$ is derived from Eq.(A14), considering $(\nabla\times\mathbf{B})\times\mathbf{B}=-\epsilon\nabla_{\perp}B_{\parallel}+O(\epsilon^2)$. Normalized closure of ion velocity is $\mathbf{u}=\hat{\mathbf{z}}\times\nabla_{\perp}\phi+u_{\parallel}\hat{\mathbf{z}}+O(\epsilon)$. Because $\kappa\sim O(\epsilon)$, the curvature is neglected in the inertia terms, and inertia terms are $\epsilon^2\mathbf{B}\cdot\nabla\times(\partial\mathbf{u}/\partial t)=\partial\nabla_{\perp}^2\phi/\partial t+O(\epsilon)$ and $\epsilon^2\mathbf{B}\cdot\nabla\times(\mathbf{u}\cdot\nabla\mathbf{u})=\hat{\mathbf{z}}\cdot\nabla_{\perp}\phi\times\nabla_{\perp}\nabla_{\perp}^2\phi+O(\epsilon)$, where Boussinesq approximation is applied. The term of anisotropic stress tensor is evaluated by $\epsilon^2\hat{\mathbf{z}}\cdot\nabla\times\nabla\cdot\pi_i\approx\epsilon^2\mu\nabla_{\perp}^4\phi$, where μ is ion viscosity. The first term of RHS of Eq.(A15) is $B^2\mathbf{B}\cdot\nabla(J_{\parallel}/B)=-\epsilon^2(\partial/\partial z-\hat{\mathbf{z}}\cdot\nabla_{\perp}A\times\nabla_{\perp})\nabla_{\perp}^2A+O(\epsilon^3)$, where $\mathbf{B}\cdot\nabla=\epsilon\left(\partial/\partial z-\hat{\mathbf{z}}\cdot\nabla_{\perp}A\times\nabla_{\perp}\right)+O(\epsilon^2)$ and $J_{\parallel}/B=-\epsilon\nabla_{\perp}^2A+O(\epsilon^2)$ are used. The second term of

RHS of Eq.(A15) is $\epsilon\mathbf{B}\times\boldsymbol{\kappa}\cdot\nabla_\perp p = -\epsilon^2\hat{\mathbf{z}}\cdot\nabla_\perp x\times\nabla_\perp p + O(\epsilon^3)$. Therefore, $O(\epsilon^2)$ component of Eq.(A15) is given by

$$\left(\frac{\partial}{\partial t}+\hat{\mathbf{z}}\cdot\nabla_\perp\phi\times\nabla_\perp\right)\nabla_\perp^2\phi = -\left(\frac{\partial}{\partial z}-\hat{\mathbf{z}}\cdot\nabla_\perp A\times\nabla_\perp\right)\nabla_\perp^2 A - \hat{\mathbf{z}}\cdot\nabla_\perp 2x\times\nabla_\perp p + \mu\nabla_\perp^4\phi. \quad \text{(A16)}$$

Secondly, the reduced parallel ion momentum equation is derived by operating $(\mathbf{B}\cdot)$ to Eq.(A14). In this operation, the $(\nabla\times\mathbf{B})\times\mathbf{B}$ term is eliminated. Considering Boussinesq-like approximation $n/n_c = 1$, the inertia term is $\epsilon^2(n/n_c)\mathbf{B}\cdot(d_i\mathbf{u}/dt) = \epsilon^2\hat{\mathbf{z}}\cdot(d_i\mathbf{u}/dt) + O(\epsilon^3) = (\partial/\partial t + \hat{\mathbf{z}}\cdot\nabla_\perp\phi\times\nabla_\perp)u_\parallel + O(\epsilon^3)$, where $u_\parallel = \hat{\mathbf{z}}\cdot\mathbf{u}$, $\mathbf{u}\cdot\nabla = \hat{\mathbf{z}}\times\nabla_\perp\phi\cdot\nabla + u_\parallel\hat{\mathbf{z}}\cdot\nabla = \hat{\mathbf{z}}\times\nabla_\perp\phi\cdot\nabla_\perp + O(\epsilon)$ and $\hat{\mathbf{z}}\cdot(\hat{\mathbf{z}}\times\nabla_\perp\phi\cdot\nabla_\perp)\mathbf{u} = \hat{\mathbf{z}}\times\nabla_\perp\phi\cdot\nabla_\perp u_\parallel$ are used. The pressure gradient term is $-\epsilon\mathbf{B}\cdot\nabla p = -\epsilon^2(\partial/\partial z - \hat{z}\cdot\nabla_\perp A\times\nabla_\perp)p + O(\epsilon^3)$. For the anisotropic stress terms, the electron component is dropped and we assume the ion component to $-\epsilon^2\mathbf{B}\cdot\nabla\pi_i = \epsilon^2\mu_\perp\nabla_\perp^2 u_\parallel + O(\epsilon^3)$. Therefore, $O(\epsilon^2)$ component of Eq.(A14) operated $(\mathbf{B}\cdot)$ is given by

$$\left(\frac{\partial}{\partial t}+\hat{\mathbf{z}}\cdot\nabla_\perp\phi\times\nabla_\perp\right)u_\parallel = -\left(\frac{\partial}{\partial z}-\hat{z}\cdot\nabla_\perp A\times\nabla_\perp\right)p + \mu_\perp\nabla_\perp^2 u_\parallel. \quad \text{(A17)}$$

Thirdly, reduced Ohm's law is derived. Normalized Ohm's law Eq.(39) is given by

$$\mathbf{E} = -\epsilon\frac{n_c}{n}\delta\nabla p - \epsilon\mathbf{v}\times\mathbf{B} + \epsilon\eta_\parallel\mathbf{J}_\parallel + \epsilon\eta_\perp\mathbf{J}_\perp - \alpha_T\delta\beta\mathbf{b}(\mathbf{b}\cdot\nabla)\left(\frac{T_e}{T_{ec}}\right), \quad \text{(A18)}$$

where $\mathbf{E} = -\epsilon\nabla\phi - \epsilon^2\partial\mathbf{A}/\partial t$. Operating $(\mathbf{B}\cdot)$, the parallel component of Ohm's law is given by

$$\mathbf{B}\cdot\left(-\epsilon\nabla\phi-\epsilon^2\frac{\partial\mathbf{A}}{\partial t}\right) = -\epsilon\frac{n_c}{n}\delta\mathbf{B}\cdot\nabla p + \epsilon\eta_\parallel B^2\frac{J_\parallel}{B} - \epsilon\alpha_T\delta\beta(\mathbf{B}\cdot\nabla)\left(\frac{T_e}{\epsilon T_{ec}}\right), \quad \text{(A19)}$$

where the anisotropic stress is neglected, because of $O(\epsilon^3)$. Terms of LHS of Eq.(A19) are $-\epsilon\mathbf{B}\cdot\nabla\phi = -\epsilon^2\partial\phi/\partial z + \epsilon^2\hat{\mathbf{z}}\cdot\nabla_\perp A\times\nabla_\perp\phi + O(\epsilon^3)$ and $-\epsilon^2\mathbf{B}\cdot(\partial\mathbf{A}\partial t) = -\epsilon^2(\partial A\partial t) + O(\epsilon^3)$. The first term of RHS of Eq.(A19) is $-(n_c/n)\delta\mathbf{B}\cdot\nabla p = -\epsilon^2\delta(\partial/\partial z - \hat{\mathbf{z}}\cdot\nabla_\perp A\times\nabla_\perp)p + O(\epsilon^3)$, considering approximation $n/n_c = 1$. The second term of RHS is $\epsilon\eta_\parallel B^2(J_\parallel/B) = -\epsilon^2\eta_\parallel\nabla_\perp^2 A + O(\epsilon^3)$. The last term of RHS is $-\epsilon\alpha_T\delta\beta(\mathbf{B}\cdot\nabla)(T_e/\epsilon T_{ec}) = -\epsilon\alpha_T\delta\beta(\partial/\partial z - \hat{\mathbf{z}}\cdot\nabla_\perp A\times\nabla_\perp)(T_e/\epsilon T_{ec}) + O(\epsilon^3)$, where it should be noted that $\beta\sim O(\epsilon)$. Therefore $O(\epsilon^2)$ component of Eq.(A19) is given by

$$\frac{\partial}{\partial t}A = -\left(\frac{\partial}{\partial z}-\hat{\mathbf{z}}\cdot\nabla_\perp A\times\nabla_\perp\right)\times\left(\phi-\delta p-\alpha_T\delta\beta\left(\frac{T_e}{\epsilon T_{ec}}\right)\right) - \eta_\parallel\nabla_\perp^2 A. \quad \text{(A20)}$$

Fourthly, the reduced continuity equation is derived. Normalized continuity equation Eq.(40) is

$$\epsilon^2\frac{d_e}{dt}\frac{n}{\epsilon n_c} + \epsilon\frac{n}{n_c}\nabla\cdot\mathbf{v} = 0. \quad \text{(A21)}$$

where $d_e/dt = \partial/\partial t + \mathbf{v}\cdot\nabla$. Operating $(\mathbf{B}\times)$ to the normalized Ohm's law Eq.(A19), we get $\mathbf{v}_\perp = (\mathbf{B}/B^2)\times\{\nabla\phi - (n_c/n)\delta\nabla p\} + \epsilon(\mathbf{B}/B^2)\times(\partial\mathbf{A}/\partial t) - \epsilon\eta_\perp(\mathbf{B}/B^2)\times\mathbf{J}$. Because $\mathbf{v}\cdot\nabla = (\mathbf{v}_\perp + v_\parallel\mathbf{b})\cdot\nabla = \hat{\mathbf{z}}\cdot\nabla_\perp\{\phi - (n_c/n)p\delta\}\times\nabla_\perp + O(\epsilon)$, the inertia term is given by $\epsilon^2 d_e(n/\epsilon n_c)/dt = \epsilon^2(\partial/\partial t + \hat{\mathbf{z}}\cdot\nabla_\perp(\phi - \delta p)\times\nabla_\perp)(n/\epsilon n_c)$. To evaluate $\nabla\cdot\mathbf{v}$, we separate $\nabla\cdot\mathbf{v} = \nabla\cdot(\mathbf{b}v_\parallel) + \nabla\cdot\mathbf{v}_\perp$. For the first term, considering $\delta\mathbf{J} = \epsilon(n/n_c)(\mathbf{u}-\mathbf{v})$, we get $\nabla\cdot(\mathbf{b}v_\parallel) = \nabla\cdot(\mathbf{b}(u_\parallel - \epsilon^{-1}(n_c/n)\delta J_\parallel)) = \epsilon(\partial/\partial z - \hat{\mathbf{z}}\cdot\nabla_\perp A\times\nabla_\perp)(u_\parallel + \delta\nabla_\perp^2 A) + O(\epsilon^2)$, where approximation $n/n_c = 1$ is used. We evaluate the second term $\nabla\cdot\mathbf{v}_\perp$ below. $\nabla\cdot\{(\mathbf{B}/B^2)\times(\nabla\phi - (n/n_c)\delta\nabla p)\} = 2\epsilon\hat{\mathbf{z}}\cdot(\nabla_\perp(\phi-\delta p)\times\nabla_\perp x) - \epsilon\hat{\mathbf{z}}\cdot\nabla_\perp\phi\times\nabla_\perp p + O(\epsilon^2)$, where approximation $n/n_c = 1$ and $\nabla\times(\mathbf{B}/B^2) = \epsilon(2\nabla_\perp x\times\hat{\mathbf{z}} - \nabla_\perp B_\parallel\times\hat{\mathbf{z}} - \hat{\mathbf{z}}\nabla_\perp^2 A) + O(\epsilon^2)$ are considered. $\epsilon\nabla\cdot\{(\mathbf{B}/B^2)\times(\partial\mathbf{A}\partial t)\} = \epsilon\partial B_\parallel/\partial t + O(\epsilon^2) = -\epsilon\partial p/\partial t + O(\epsilon^2)$, where $B_\parallel = -p + O(\epsilon)$ is assumed, considering the relation $\nabla_\perp(B_\parallel + p)\sim O(\epsilon)$. $\epsilon\eta_\perp\nabla\cdot\{(\mathbf{B}/B^2)\times\mathbf{J}\} = -\epsilon\eta_\perp\nabla_\perp^2 B_\parallel + O(\epsilon^2) = \eta_\perp\epsilon\nabla_\perp^2 p + O(\epsilon^2)$. Then we can evaluate $\nabla\cdot\mathbf{v}_\perp = 2\epsilon\hat{\mathbf{z}}\cdot\nabla_\perp(\phi-\delta p)\times\nabla_\perp x - \epsilon(\partial/\partial t + \hat{\mathbf{z}}\cdot\nabla_\perp\phi\times\nabla_\perp)p - \epsilon\eta_\perp\nabla_\perp^2 p + O(\epsilon^2)$. Considering approximation $n/n_c = 1$ for the second term of Eq.(A21), the reduced continuity equation is given by

$$\left(\frac{\partial}{\partial t}+\hat{\mathbf{z}}\cdot\nabla_\perp\phi\times\nabla_\perp\right)\left(\frac{n}{\epsilon n_c}\right) + \left(\frac{\partial}{\partial t}+\hat{\mathbf{z}}\cdot\nabla_\perp\phi\times\nabla_\perp\right)p = \hat{\mathbf{z}}\cdot\nabla_\perp 2x\times\nabla_\perp(\phi-\delta p) - \left(\frac{\partial}{\partial z}-\hat{\mathbf{z}}\cdot\nabla_\perp A\times\nabla_\perp\right)(u_\parallel + \delta\nabla_\perp^2 A) + \eta_\perp\nabla_\perp^2 p. \quad \text{(A22)}$$

where $\delta\hat{\mathbf{z}}\cdot\nabla_\perp p\times\nabla_\perp(n/\epsilon n_c)$ by the time derivative of electron density is neglected for the energy conservation.

Fifthly, the reduced electron temperature equation is derived. Normalized electron temperature equation Eq.(34) is given by

$$\epsilon^2\frac{3}{2}\frac{n}{n_c}\frac{d_e}{dt}\left(\frac{T_e}{\epsilon T_{ec}}\right) - \epsilon^2\frac{T_e}{T_{ec}}\frac{d_e}{dt}\left(\frac{n}{\epsilon n_c}\right) = -\frac{1}{n_c T_{ec}}\frac{1}{v_A}\nabla\cdot\mathbf{q}. \quad \text{(A23)}$$

with

$$
\begin{aligned}
&-\frac{1}{n_c T_{ec}}\frac{1}{v_A}\mathbf{q} \\
&=\epsilon^2\chi_{\parallel}\mathbf{b}\left(\mathbf{b}\cdot\nabla\right)\left(\frac{T_e}{\epsilon T_{ec}}\right)+\epsilon^2\chi_{\perp}\left(\nabla-\mathbf{b}\left(\mathbf{b}\cdot\nabla\right)\right)\left(\frac{T_e}{\epsilon T_{ec}}\right) \\
&-\frac{5}{2}\epsilon^2\delta p\mathbf{b}\times\nabla\left(\frac{T_e}{\epsilon T_{ec}}\right)+\alpha_T\delta\frac{T_e}{T_{ec}}\mathbf{J}_{\parallel}. \qquad \text{(A24)}
\end{aligned}
$$

In heat flux term, we have $\nabla\cdot(\mathbf{b}\cdot\nabla)(T_e/\epsilon T_{ec}) = \epsilon^2(\partial/\partial z-\hat{z}\cdot\nabla_\perp\phi\times\nabla_\perp)^2(T_e/\epsilon T_{ec})+O(\epsilon^3)$ and $\nabla\cdot(\nabla-\mathbf{b}(\mathbf{b}\cdot\nabla))(T_e/\epsilon T_{ec}) = \nabla_\perp^2(T_e/\epsilon T_{ec})+O(\epsilon)$. Using approximation $T_e/T_{ec}=1$, we obtain $\nabla\cdot\{\alpha_T\delta(T_e/T_{ec})\mathbf{J}_{\parallel}\} = -\epsilon^2\alpha_T\delta\nabla_{\parallel}\nabla_\perp^2 A+O(\epsilon^3)$. Considering approximation $T_e/T_{ec}=n/n_c=1$ on the LHS of Eq.(A23), we get the reduce electron temperature equation

$$
\begin{aligned}
&\frac{3}{2}\left(\frac{\partial}{\partial t}+\hat{\mathbf{z}}\cdot\nabla_\perp\phi\times\nabla_\perp\right)\left(\frac{T_e}{\epsilon T_{ec}}\right) \\
&-\left(\frac{\partial}{\partial t}+\hat{\mathbf{z}}\cdot\nabla_\perp\phi\times\nabla_\perp\right)\left(\frac{n}{\epsilon n_c}\right) \\
&=-\alpha_T\delta\nabla_{\parallel}\left(\nabla_\perp^2 A\right)+\epsilon^2\chi_{\parallel}\nabla_{\parallel}^2\left(\frac{T_e}{\epsilon T_{ec}}\right)+\chi_\perp\nabla_\perp^2\left(\frac{T_e}{\epsilon T_{ec}}\right). \qquad \text{(A25)}
\end{aligned}
$$

where $-\epsilon^2(3/2)\delta[p,T_e/\epsilon T_{ec}]+\epsilon^2\delta[p,n/\epsilon n_c]+\epsilon^2(5/2)\delta\nabla\cdot\{p\mathbf{b}\times\nabla(T_e/\epsilon T_{ec})\}$ by convective derivatives and heat flux term is neglected for the energy conservation.

Finally, T_e and n are normalized as $\beta T_e/\epsilon T_{ec}\to T$ and $\beta n/\epsilon n_c\to n$. The reduced set derived above is summarized.

$$
\begin{aligned}
\frac{D}{Dt}\nabla_\perp^2\phi &= \nabla_{\parallel}j_{\parallel}-[\Omega,p]+\mu\nabla_\perp^4\phi, && \text{(A26)}\\
\frac{D}{Dt}u_{\parallel} &= -\nabla_{\parallel}p+\mu_\perp\nabla_\perp^2 u_{\parallel}, && \text{(A27)}\\
\frac{\partial}{\partial t}A &= -\nabla_{\parallel}\left(\phi-\delta p-\alpha_T\delta T\right)+\eta j_{\parallel}, && \text{(A28)}\\
\frac{D}{Dt}n+\beta\frac{D}{Dt}p &= \beta[\Omega,\phi-\delta p]-\beta\nabla_{\parallel}\left(u_{\parallel}-\delta j_{\parallel}\right) \\
&\quad +\eta_\perp\beta\nabla_\perp^2 p, && \text{(A29)}\\
\frac{3}{2}\frac{D}{Dt}T-\frac{D}{Dt}n &= \alpha_T\delta\beta\nabla_{\parallel}j_{\parallel}+\epsilon^2\chi_{\parallel}\nabla_{\parallel}^2 T+\chi_\perp\nabla_\perp^2 T. && \text{(A30)}
\end{aligned}
$$

where $D/Dt=\partial/\partial t+[\phi,]$, $\nabla_{\parallel}=\partial/\partial z-[A,]$, $[f,g]=\hat{\mathbf{z}}\cdot\nabla_\perp f\times\nabla_\perp g$, $j_{\parallel}=-\nabla_\perp^2 A$ $\alpha_T=0.71$ and $\Omega=2x$ $(\nabla\Omega=-2(\hat{\mathbf{b}}\cdot\nabla)\hat{\mathbf{b}})$.